



Supplementary Materials for

Persistent effect of El Niño on global economic growth

Christopher W. Callahan and Justin S. Mankin

Corresponding author: Christopher W. Callahan, christopher.w.callahan.gr@dartmouth.edu

DOI: 10.1126/science.adf2983

The PDF file includes:

Materials and Methods
Supplementary Text
Figs. S1 to S17
Tables S1 to S7
References

Materials and Methods

Data

We use observational climate data from multiple sources: Monthly mean sea surface temperatures (SST) from the HadISST dataset (49), monthly mean atmospheric temperatures from the Berkeley Earth dataset (50), and monthly total precipitation data from the Global Precipitation Climatology Center (51). Temperature and precipitation are aggregated to population-weighted country-level means using year-2000 population data from the Gridded Population of the World (52). We use population weighting to ensure that the spatial aggregation captures climate fluctuations that affect people and economic activity.

We use country-level economic data from the Penn World Tables version 10.0 (53), specifically Gross Domestic Product (“RGDPNA”) (in 2017-equivalent dollars) and population (“POP”) for all countries of the world. GDP per capita (GDPpc) is calculated as GDP divided by population. Growth for each year is calculated as the fractional GDPpc change relative to the previous year. Because macroeconomic data may contain measurement error (54), we also repeat the analysis using data from the World Bank World Development Indicators (55), finding similar results (Fig. S4).

The time period of analysis for both the teleconnection calculations and regression analysis is 1960-2019, so all observational economic and climate data is limited to that time period.

Climate model data come from the sixth phase of the Climate Model Intercomparison Project (56) (CMIP6). We use monthly SST, monthly atmospheric temperature, and daily precipitation data over 1850-2099 from the historical experiment and the four Tier 1 experiments from the Scenario Model Intercomparison Project (57). These four experiments—SSP1-2.6, SSP2-4.5, SSP3-7.0, and SSP5-8.5—span a range of plausible policy futures, from aggressive mitigation (SSP1-2.6) to high emissions (SSP5-8.5) (57, 58). Global mean temperatures rise by ~1.2 °C by 2081-2100 relative to 1995-2014 in the SSP1-2.6 scenario, 2.1 °C in SSP2-4.5, 3.2 °C in SSP3-7.0, and 4 °C in SSP5-8.5 (58). Not all models have data available for each experiment, so differences across the experiments are due both to differences in forcing and differences in the sampling of model structure (Tables S3-S6). All climate model data is regressed to a 2°-by-2° grid, using bilinear interpolation from Python’s “xarray” package (59).

ENSO indices

We use the “E-index” and “C-index” to represent ENSO (9, 27, 36, 60, 61). The E-index represents eastern Pacific El Niño events and captures the nonlinear processes that generate skewness in eastern Pacific SSTs, whereby El Niño events are stronger than La Niña events (9, 27). The E-index is a combination of the first two principal components (PCs) of an empirical orthogonal function (EOF) analysis applied to Pacific SSTs (36) over 20 °S – 20 °N and 140 °E – 80 °W, specifically as $E = (PC_1 - PC_2)/\sqrt{2}$. We calculate the E-index in observations using linearly detrended SST anomalies referenced to 1960-2019 long-term monthly means. We then average the E-index over winter (December-February, DJF), to focus on the season in which ENSO peaks (62); the E-index in year t is therefore defined as the average of the December E-index from year $t-1$ and the January and February indices from year t .

The C-index (27) is a companion index to the E-index and is calculated as $C = (PC_1 + PC_2)/\sqrt{2}$. The C-index represents central Pacific La Niña and El Niño events, where La Niña events tend to be stronger than El Niño events. Positive E-index values represent an eastern Pacific El Niño event and negative C-index values represent a central Pacific La Niña event. The

E-index and C-index are orthogonal by construction (27), allowing us to include them both in a regression model without a concern for collinearity.

To assess the sensitivity of our results to these indices, we also calculate the Niño3 index, defined as linearly detrended SST anomalies averaged over 5 °S – 5 °N and 150 °W – 90 °W. The Niño3 index yields similar, though slightly weaker, results to the E-index (Fig. S4) since it corresponds to eastern Pacific conditions but does not distinguish the spatial structures of El Niño and La Niña.

We calculate the DJF E- and C-indices similarly in the CMIP6 models, using quadratically detrended (9) SST anomalies referenced to monthly means from 1850-2014.

Country-level ENSO teleconnections

Our analysis uses a country-specific teleconnection metric to quantify heterogeneity in growth responses according to a country's geophysical connection to ENSO. To calculate the teleconnection, we first standardize monthly country-level mean temperature and total precipitation by subtracting the long-term (1960-2019) monthly mean and dividing by the long-term monthly standard deviation. We then linearly detrend these standardized anomalies separately for each month to remove the effects of warming and low-frequency climate variability.

Next, we correlate these standardized temperature and precipitation time series with the DJF E-index separately for each month m and each country i . El Niño events begin and grow in year $t-1$, peak in the winter, and then decay in the spring and summer of year t , so we allow the DJF E-index to affect both the preceding (beginning just after the “spring predictability barrier” in June of $t-1$) and following years (ending in August of year t) (Fig. S1). We use partial correlations to control for precipitation when analyzing temperature and vice versa to control for the covariance between temperature and precipitation.

This calculation yields a distribution of 15 correlation coefficients (one per month from June of year $t-1$ through August of year t) for each country, separately for temperature and precipitation. We then take the three-month running mean of these coefficients across the 15 months to smooth out random variation and account for multiple months of exposure to ENSO. Finally, we take the maximum (absolute) correlation coefficients from these running means for both temperature and precipitation and add them together to calculate each country's E-index teleconnection τ^E . We use absolute values to allow the distinct effects of temperature and precipitation teleconnections to be additive, but our results are robust to considering both positive and negative precipitation teleconnections separately (Fig. S5).

This teleconnection metric estimates the degree to which each country's climate is influenced by ENSO, accounting for: (1) the effects of both temperature and precipitation; (2) multiple sustained months of exposure to ENSO; and (3) the varied timescales on which teleconnections may manifest. Additionally, this strategy allows teleconnections to be defined continuously rather than separating teleconnected and non-teleconnected countries based on arbitrary significance thresholds (8) or previously defined climate zones (19, 20). Fig. S2 shows the steps in this teleconnection calculation, and we perform the same analysis with the C-index to calculate C-index teleconnections (τ^C).

Econometric analysis

The goal of our analysis is to quantify the multi-year effect of ENSO on economic growth. This task requires us to separate ENSO from the other constant and time-varying factors that

affect economic growth. We use a distributed lag regression model, estimated with Ordinary Least Squares, to estimate the effects of eastern Pacific El Niño (the E-index) and central Pacific La Niña (the C-index) on growth:

$$g_{it} = \sum_{L=0}^j [\beta_L E_{t-L} + \Theta_L E_{t-L} * \tau_i^E + \Phi_L C_{t-L} + \Psi_L C_{t-L} * \tau_i^C] + \mu_i + \epsilon_{it} \quad (1)$$

Here, g refers to GDPpc growth in country i in time t , E refers to the E-index in year t , and C refers to the C-index in year t . μ is a country fixed effect, which controls for average differences between countries such as geography and ensures that our results are identified using within-country variation in growth. L is the lag at which the coefficient is estimated. The interactions of E with τ^E and C with τ^C allow the effect of ENSO to differ between countries based on how strongly coupled each country's climate is to ENSO.

The inclusion of lagged terms from years L to j allows us to distinguish between level and growth effects on the economy. If the effect of El Niño only falls on income levels, then a shock in year t will be recovered in year $t+1$ as countries rebound to their original income trajectory, meaning that year $t+1$ will see an abnormally high growth rate. If, instead, El Niño affects the underlying capacity of the economy to grow, then the years following an event should show either persistent declines in growth or no change. As such, our analysis focuses on the cumulative coefficients Ω , which represent the accumulated effect of ENSO in the years after an event. The interaction of E with country-specific teleconnections τ^E allows us to calculate unique cumulative effects for each country i and lag length L :

$$\Omega_{iL} = \sum_{L=0}^j [\beta_L + \Theta_L * \tau_i^E] \quad (2)$$

If Ω_{iL} is indistinguishable from zero, then we cannot reject the hypothesis that El Niño has only level effects; growth effects are identified if Ω_{iL} is significantly different from zero ($p < 0.05$). Note that the E-index is not highly correlated with itself across lag lengths (Table S7), meaning that including multiple lags in a single model should not generate multicollinearity.

The identifying variation in our model comes from stochastic and unpredictable (30, 63) shifts in SSTs from year to year, along with the differential effects of those SSTs depending on teleconnection strength. The E- and C-indices are constant throughout space within a given year, raising the concern that other time-varying confounders could be correlated with ENSO and generating spurious results. A typical strategy in empirical climate-economy studies is to include both unit and time fixed effects in regression models (64), which separate local weather variation from both time-invariant average conditions and global time-varying shocks. However, because the E- and C-index terms in Eqn. 1 would be collinear with the year fixed effect, we cannot estimate our main specification with year effects.

We do, however, show results from several alternative models that separate the influence of ENSO from time-varying confounders. First, adding linear or linear and quadratic country-level time trends to control for secular trends in technology or demographics does not alter our results (Fig. S4). Second, bootstrap resampling by year permutes the years in the regression model and ensures that no single year has a disproportionate influence on the results (Fig. S3). Third,

dropping 1983 and 1998 from our data, which were major El Niño events that coincided with financial crises in tropical countries, reduces the magnitude of the effects we find by ~12% but does not alter their statistical or economic significance (Fig. S4). Fourth, we define a unique spatiotemporally varying ENSO index for each country and year by multiplying E_t by τ_i^E . Because this index differs across countries within years, we can estimate the model with country and year fixed effects, and we find negative effects that exceed the results of our main model (Fig. S7). For example, this model predicts that Peru experiences an 8.7-p.p. decline in growth five years after an El Niño, compared to 6.2 p.p. from our original model. Finally, we estimate a discretized version of our main model, where we defined “untreated” countries as countries with $\tau_i^E < 0.5$ and “treated” countries as countries with $\tau_i^E > 0.5$. This allows us to estimate the model with country and year fixed effects, interpreting the discretized interaction term as the effect of ENSO on treated countries. In this case, we find that treated countries experience >3-p.p. declines in growth five years after El Niños, which exceeds the 2.3-p.p. average loss for countries with $\tau_i^E > 0.5$ from our main model (Fig. S7). The inclusion of year fixed effects in these latter two models, along with the other checks we show, supports our conclusion that our results are not driven by time-varying confounders.

We estimate confidence intervals by bootstrapping ($N = 1,000$), with countries resampled from a uniform distribution with replacement. Countries are sampled as a block to account for within-country autocorrelation (65). However, alternative bootstrapping schemes yield similar results, such as sampling by year globally or within continents to account for spatial correlation in growth, sampling by continent to account for simultaneous spatial and temporal correlation, and sampling by five-year blocks to account for spatial and short-term temporal correlation (65) (Fig. S3). Multiple forms of clustered parametric standard errors, which are robust to both spatiotemporal autocorrelation in errors and heteroskedasticity across clusters, do not reduce the statistical significance of our results (Table S1, S2).

We remove growth values from our sample that are above 18% or below -18%, approximately the 3σ range. We drop 146 values because of this choice, less than 2% of the sample. Including these values does not reduce the average effect, but it does increase the uncertainty (Fig. S4), so we drop these outliers while noting that our results would be similar if we included them.

When we estimate separate responses for high-income and low-income countries (Fig. S4), we use the World Bank’s income classifications, grouping low and lower-middle income countries together as well as high and higher-middle income countries. Again, the results accord with our main model.

Other time series analysis tools have been used to assess the effect of ENSO such as vector autoregression (VAR) models (18, 21–23) or local projections (18). We use a distributed lag (DL) model for two reasons. Firstly, DL models have been widely used in the empirical climate-economy literature (13, 15, 66, 67), so our approach is consistent with this work. Secondly, VAR models are primarily used in macroeconomic settings where endogeneity is at issue (68). Because ENSO is plausibly exogenous to country-level growth rates, we adopt the more parsimonious DL model.

Synthetic data simulations

Estimating the effect of El Niño with models that include 14 or more lags results in unstable coefficients and confidence intervals that include zero (Fig. S8). Two plausible interpretations of this result are: (1) that there is no statistically significant growth effect of El Niño after 14 years;

or (2) that there is a permanent growth effect, but models with many lags cannot confidently identify this effect due to the reduced sample size and increased number of parameters being estimated simultaneously.

To examine this issue, we use a perfect model framework where we impute a known El Niño effect to synthetic growth data and then estimate the regression on that data to assess whether we can recover the effect. We construct growth as the combination of a first-order autocorrelated process (AR(1)) with Gaussian noise of mean 0 and s.d. 0.05, a linear trend randomly chosen from a Gaussian distribution of mean 0 and s.d. 0.2 (in p.p. per year), and an El Niño effect. The AR(1) coefficient is set to 0.1, within the range of AR(1) coefficients from the data, and the distribution of trends we choose from is also similar to the distribution of country-level growth trends from the data (Fig. S15).

We then create a “true” effect of ENSO on growth and attempt to recover it with the DL model. This predetermined ENSO effect is ultimately arbitrary, but we choose country-level effects that are similar in magnitude to the effects we find in our main regression. We set these effects to accumulate over the first 5 years and plateau at that 5-year value permanently. The non-interacted effect of E is set to sum to 3 p.p. per s.d. and the interaction coefficient with τ is set to sum to -6 p.p. per s.d., meaning that a country with $\tau^E = 1.0$ experiences a cumulative effect of -3.0 p.p. per s.d. ($3 + 1.0 * -6$).

We then fit Eqn. 1 using this synthetic growth data and the actual E -index and τ^E values, using between 5 and 18 lags in the regression (beyond 18 lags, the coefficients become undefined as the degrees of freedom decrease). We repeat this entire process 1,000 times for each number of lags, keeping the set El Niño effect constant. Fig. S8 shows the results from these estimations for one example teleconnection value ($\tau^E = 1.0$). These models are generally unbiased, with the central estimate matching the imputed effect. However, confidence intervals steadily grow as lags are added. With 14 or more lags, the coefficients become statistically insignificant. These results demonstrate that even with a known permanent effect of El Niño, estimating additional lag terms induces sufficient uncertainty to yield insignificant coefficients. To assume that El Niño has no effect in the 14-lag model therefore risks a Type II error. That being said, as a conservative choice in our historical attribution and in our damage projections, we only allow the effects to be partially persistent rather than permanently persistent (see *Economic damages from changes to ENSO*). In our attribution of the costs of the 1982-83 and 1997-98 events, we estimate costs accumulating to 5 years after the event. In our projections, we allow effects to accumulate to 14 years, the maximum length we can confidently identify effects from the observational data (Fig. S8). In a sensitivity test, we allow the effects to be permanent (Fig. S13).

Economic damages from historical extreme El Niño events

The regression coefficients derived from Eqn. 1, β and θ , provide estimates of the change in economic growth for a 1-s.d. change in the E -index. These coefficients can then be applied to actual and hypothetical E -index time series to calculate the growth effects of specific historical El Niño events. Here we focus on the two major El Niño events of 1982-83 and 1997-98. We develop “counterfactual” E -index time series wherein these events did not occur by setting the corresponding E -index values (1983 and 1998) to zero. We then apply the regression coefficients to the actual and counterfactual time series to calculate the growth difference between them over the five years after the event. Formally, if E^0 represents the observed E -index in the year of the

event (t), and E^{CF} represents the counterfactual E-index in that year, we calculate the growth change in country i from year t through year $t+L$ as:

$$\Delta g_{i(t+L)} = [\beta_L E_t^{CF} + \Theta_L E_t^{CF} * \tau_i^E] - [\beta_L E_t^O + \Theta_L E_t^O * \tau_i^E] \quad (3)$$

We add these growth change values to the observed growth data, yielding a counterfactual growth time series, and we integrate counterfactual growth to calculate counterfactual income from the year of the event to 5 years after the event. Losses due to each event are calculated as the difference between observed and counterfactual income. Details of this procedure can be found in Difffenbaugh and Burke (69).

Note that E^{CF} is zero in our analysis, so the first bracketed term on the right-hand-side of Eqn. 3 is zero, but we provide the full equation because it generalizes to other counterfactual E-index values.

The above analysis only incorporates reductions in growth due to the El Niño events. However, because El Niño events can dynamically trigger La Niña events (34), which have beneficial effects (Fig. S10), a full accounting of the effects of El Niño should incorporate these offsetting beneficial events. The 1982-83 El Niño may have triggered the La Niña of 1984-85 (while the C-index was only -0.07 in 1984, it was -1.1 in 1985), and the 1997-98 El Niño may have triggered the major La Niña of 1999-2000 (the C-index was -2.1 in 1999 and -2.0 in 2000). We incorporate these beneficial effects for both El Niño events by setting the C-index values for the following two years (i.e., 1999 and 2000 in the case of the 1998 El Niño) to zero and calculating the growth difference between the actual and counterfactual C-index time series. The total growth change over the five years following the El Niño event is therefore the reduction due to the El Niño event plus the increase due to the following La Niña events.

For both events, we limit our analysis to countries with continuous GDPpc data since 1982 to ensure that the same countries are included in both calculations. This restriction means that nations with short GDPpc records (e.g., post-Soviet nations like Ukraine) are not included in these calculations.

Climate model selection

Many climate models do not realistically represent the physical processes that drive ENSO (70–72). To ensure that our projections are physically realistic, we filter the simulations we use based on criteria set out in previous studies (9, 36, 72). We calculate a parameter known as α from each model, which is the quadratic coefficient on the relationship between the first and second principal components from the EOF analysis used to calculate the E-index and C-index (72) (see *ENSO indices*).

The observed value of α is -0.34, indicating a strong nonlinearity in the principal component space and a strong differentiation between eastern Pacific and central Pacific El Niño events. Models which simulate an α value closer to the observed value also more effectively represent the variance and skewness in SST anomalies, as well as the distinct eastern and central Pacific El Niño phases (9, 72). We follow Cai et al. (9) in selecting all models with α at least 50% of the observed value, meaning -0.17 or less. Tables S3-S6 show the total and selected realizations for each experiment. We also test the sensitivity of our results to using only one realization from each model (Fig. S13).

ENSO amplitude and teleconnections in climate models

We define ENSO amplitude as the standard deviation of the quadratically detrended E-index (9, 42). We calculate each climate model simulation’s amplitude in the historical period, which we define as 1940-2019 to parallel the observational data, and in the future, which we define as 2020-2099. The 1940-2019 historical period is chosen so that the historical period is the same length as the future period.

We calculate model-based ENSO teleconnections using the same method as the observations. We perform this calculation separately for the historical and future periods, standardizing and linearly detrending each country’s temperature and precipitation time series independently for each period. This method removes mean shifts due to global warming or low-frequency variability and allows us to isolate the interannual signal of ENSO.

Economic damages from changes to ENSO

Calculating economic damages from warming-driven ENSO changes requires a counterfactual world where ENSO evolves without rising temperatures. We calculate the counterfactual ENSO time series for each simulation by re-scaling its future time series to have the amplitude that simulation had in the historical period. For example, if E-index amplitude increases by 20% for a given model realization, we calculate its counterfactual E-index time series by multiplying its future time series by 0.8 (i.e., $0.8 = 1 - 0.2$). This method preserves the particular sequence of El Niño and La Niña events in the future, since this sequence is assumed to be unforced (Fig. S12), but eliminates the forced change in ENSO amplitude.

We calculate counterfactual ENSO teleconnections with a similar “delta method.” For each country in each model, we calculate the change in teleconnection value between the historical and future simulations. We then add this change to each country’s observed teleconnection value to implicitly bias-correct the model output. The “counterfactual” teleconnections are thus equal to the observed values and the “future” teleconnections are the observed-plus-change values.

We then calculate the economic effects of changes to ENSO by comparing the future and counterfactual time series and teleconnections from each model. For each year t between 2020 and 2099, we calculate the growth change from year t to year $t+5$ as the difference between the future and counterfactual time series and teleconnections:

$$\Delta g_{i(t+L)} = [\beta_L E_t^{CF} + \Theta_L E_t^{CF} * \tau_i^{CF}] - [\beta_L E_t^F + \Theta_L E_t^F * \tau_i^F] \quad (4)$$

Here, E^F refers to the future E-index time series and E^{CF} refers to the counterfactual E-index time series. Similarly, τ^F refers to future teleconnections and τ^{CF} refers to counterfactual teleconnections. This calculation yields a growth change time series where each value is the combined effect of the contemporaneous and lagged effects. We then calculate economic growth caused by changes in ENSO by subtracting these growth change values from the SSP income growth projections and integrating growth to calculate income; the new time series represent the deviations from the SSP baselines caused by changes in ENSO amplitude. Damages are calculated as the difference between this new time series and the SSP baseline. Details of this procedure can be found in Burke et al. (13). We perform an analogous calculation using the C-index time series and teleconnections to calculate C-index damages.

We note that this procedure calculates counterfactual income as accumulated over the entire 21st century, rather than preceding specific events such as in Fig. 2. This distinction is because these two methods are aimed at answering different questions. In Fig. 2, we are interested in the

effects of specific El Niño events, whereas in Fig. 4, we are interested in the accumulated effect of human-caused changes in ENSO over the 21st century.

Finally, given the rebound effects observed after ~10 lags, as well as the large uncertainties in models including longer lags (Fig. S8), we adopt a conservative approach to damage persistence in these calculations. Because we cannot confidently identify permanent effects after 14 years, we allow the growth effect of ENSO to rebound to zero 14 years after the event, meaning that each El Niño affects the global economy for 15 years total (14 lags plus a contemporaneous effect). We do this by applying Eqn. 4 for the first six years (year 0 through year 5) using the coefficients from the main 5-lag model, then allowing the effect to plateau for years 6 through 8, then reversing those coefficients and allowing economies to rebound from years 9 through 14. Thus, while we prevent El Niño events from having more than 15 years of an effect, this does not mean that their effect is zero; an affected country has lost substantial economic output during those 15 years that is never recovered. Fig. S16 illustrates this schematically. In a sensitivity analysis, we show results if we assume that damages are permanent and never recovered, a choice which yields substantially greater losses as well as greater uncertainty in those losses (Fig. S13d).

Supplementary Text

Regression-based teleconnections

Our main analysis uses a correlation coefficient to calculate teleconnections, but we also assess the sensitivity of this choice by using partial regression coefficients instead. Using a regression coefficient leads Peru and Ecuador to be strong outliers from the rest of the distribution (fig. S4e), with values at or above 2. Estimating the growth regression with these values leads to large uncertainties as Peru and Ecuador have an outsized influence on the regression (fig. S4e), so the correlation coefficient is a more stable metric for use in the growth regression. However, we emphasize that the effect of El Niño is still strong and statistically significant when using regression coefficients (Fig. S4e), so our results are not an artifact of the choice to use the correlation coefficient.

Temperature- or precipitation-based teleconnections

Our main analysis defines teleconnections using the combination of temperature and precipitation correlations. We can also define teleconnections solely based on the temperature or precipitation portions of the calculation, similar to previous studies that have focused on temperature to define teleconnections (6, 8). Results for this sensitivity analysis are shown in Fig. S5. The temperature-based estimate is similar to that from both temperature and precipitation, but the effect is weaker with precipitation alone. Our interpretation is that aggregating the data to the monthly time scale and country spatial scale dampens the signal of precipitation more than it does temperature. Consistent with this interpretation, empirical climate-economy studies tend to find little effect of precipitation on country-level growth (13, 16).

Cumulative teleconnections

By using the maximum of three-month running means, our main teleconnection analysis focuses on countries' short-term extreme exposure to ENSO rather than capturing cumulative exposure over the entire ENSO life cycle. An alternative teleconnection metric which uses the

sum of statistically significant ($p < 0.05$) correlation coefficients across the 15 months for each country yields very similar results, with high correlations between this and our original metric and nearly identical marginal growth effects (fig. S5). This analysis implies that focusing on the few months of maximum exposure is sufficient to capture the effects of ENSO on economies broadly.

Heterogeneity in historical teleconnections

Our main analysis treats teleconnections as constant in time in the observational period. However, sampling variability and changes in ENSO behavior (among other things) may result in temporal heterogeneity in teleconnections. Fig. S17 shows teleconnections calculated in rolling 30-windows over the historical period. Temporal variation is apparent, at least partly due to the shorter time period used to calculate these teleconnections. However, the distribution of teleconnection values is relatively stable, and the average country experiences temporal variation of only about 13% of its mean value. As such, we use the teleconnection values calculated across the entire time period in our main analysis, though we do allow teleconnections to change with forcing in our climate model analysis.

Finally, a key consideration in empirical climate-economy studies is the need to aggregate physical variables to the country scale, which is not a geophysically meaningful scale. To understand the implications of this aggregation, we re-calculate E-index teleconnections at the gridded scale (fig. S17). Teleconnections can vary across grid cells, but the average country only experiences within-country spatial variation of about 11% of its mean teleconnection value (fig. S17). Furthermore, population-weighted country-average grid-cell teleconnection values are similar to the original teleconnection values calculated from country-average temperature and precipitation (fig. S17), implying that subnational spatial variation in ENSO teleconnections does not substantially affect our results.

Relationship between our work and recent differences-in-differences literature

Our empirical framework is very similar to typical “differences-in-differences” (DID) approaches in economics, involving a treatment variable that varies over time (E and C) and a cross-sectional variable that denotes treatment status (τ). A series of recent papers have illustrated problems with traditional DID approaches, especially when treatment effects are heterogeneous in time and space and treatment timing is staggered (73–75). This type of research design can produce inappropriate comparisons between already treated and newly treated units, resulting in average treatment effect estimates that differ in magnitude and sign from the true effects. While novel estimators have been proposed to avoid these problems (76–78), this literature is still emerging and it is not clear that such estimators are designed for settings with continuous treatments that vary year-to-year and have dynamic effects (79). In lieu of using an alternative estimator, we run several robustness tests to examine the heterogeneity of the effects of ENSO over time and space, which can indicate whether our results are biased by this heterogeneity (80). We estimate the effect in rolling thirty-year windows over the 1960–2019 sample period, after dropping individual countries, and after dropping individual years (Fig. S6). In all cases, these estimates are quite similar to our main effect, indicating that unmodeled treatment effect heterogeneity should not pose a threat to our main analysis.

Value of climate model selection

Our climate model selection criterion preserves the benefit of a multi-model ensemble, allowing us to sample structural uncertainty in model representation of ENSO as well as initial-condition uncertainty, while incorporating information about model skill (81). Treating all simulations in a multi-model ensemble equally has been criticized for assuming that all simulations are independent samples that represent the climate system with equal skill (82), especially since CMIP is an ensemble of opportunity rather than a systematic sampling of uncertainty space. Our consideration of model skill provides an ensemble estimate that is likely more accurate than could be achieved without such consideration. Other methods such as bias correction (83, 84) could also improve ensemble skill, but we use the simpler selection criterion based on α given its consistency with the E- and C-indices and its use in the ENSO modeling community.

Sensitivity of damages calculation to alternative choices

We incorporate both amplitude and teleconnection changes in our damage projections. Holding teleconnections constant reduces both the magnitude and uncertainty of the damage projections, though they remain negative on average and negatively skewed (fig. S13). Further, a key assumption in these calculations is that the β and θ coefficients (Eqn. 1) remain consistent at a given teleconnection level between the past and future, though individual countries' actual teleconnections may change. This assumption would be violated if societies undertook adaptation measures in response to changes in ENSO amplitude or teleconnections to reduce their sensitivity to ENSO, which is why the need for increased adaptation is a key theme in our results.

Finally, our damages calculations use as many simulations from each model as possible (Tables S3-S6) to sample both model structural differences and differences in outcomes due to internal climate variability. Using only the first simulation from each model can generate different results; for example, the SSP5-8.5 simulation yields benefits and SSP1-2.6 yields stronger losses. However, we emphasize that—conditional on our model selection criterion—all selected simulations from a given model are physically plausible given the forcing and boundary conditions. Therefore, the results we present in Fig. 4 are a more complete accounting of the possible effects of ENSO changes.

References and Notes

1. M. J. McPhaden, S. E. Zebiak, M. H. Glantz, ENSO as an integrating concept in earth science. *Science* **314**, 1740–1745 (2006). [doi:10.1126/science.1132588](https://doi.org/10.1126/science.1132588) Medline
2. J. Bjerknes, Atmospheric teleconnections from the equatorial pacific. *Mon. Weather Rev.* **97**, 163–172 (1969). [doi:10.1175/1520-0493\(1969\)097<0163:ATFTEP>2.3.CO;2](https://doi.org/10.1175/1520-0493(1969)097<0163:ATFTEP>2.3.CO;2)
3. S.-W. Yeh, W. Cai, S.-K. Min, M. J. McPhaden, D. Dommenget, B. Dewitte, M. Collins, K. Ashok, S.-I. An, B.-Y. Yim, J.-S. Kug, ENSO atmospheric teleconnections and their response to greenhouse gas forcing. *Rev. Geophys.* **56**, 185–206 (2018). [doi:10.1002/2017RG000568](https://doi.org/10.1002/2017RG000568)
4. T. W. Corringham, D. R. Cayan, The effect of El Niño on flood damages in the western United States. *Weather Clim. Soc.* **11**, 489–504 (2019). [doi:10.1175/WCAS-D-18-0071.1](https://doi.org/10.1175/WCAS-D-18-0071.1)
5. F. J. Magilligan, P. S. Goldstein, El Niño floods and culture change: A late Holocene flood history for the Rio Moquegua, southern Peru. *Geology* **29**, 431–434 (2001). [doi:10.1130/0091-7613\(2001\)029<0431:ENOFAC>2.0.CO;2](https://doi.org/10.1130/0091-7613(2001)029<0431:ENOFAC>2.0.CO;2)
6. S. M. Hsiang, K. C. Meng, Tropical economics. *Am. Econ. Rev.* **105**, 257–261 (2015). [doi:10.1257/aer.p20151030](https://doi.org/10.1257/aer.p20151030)
7. T. Iizumi, J.-J. Luo, A. J. Challinor, G. Sakurai, M. Yokozawa, H. Sakuma, M. E. Brown, T. Yamagata, Impacts of El Niño Southern Oscillation on the global yields of major crops. *Nat. Commun.* **5**, 3712 (2014). [doi:10.1038/ncomms4712](https://doi.org/10.1038/ncomms4712) Medline
8. S. M. Hsiang, K. C. Meng, M. A. Cane, Civil conflicts are associated with the global climate. *Nature* **476**, 438–441 (2011). [doi:10.1038/nature10311](https://doi.org/10.1038/nature10311) Medline
9. W. Cai, G. Wang, B. Dewitte, L. Wu, A. Santoso, K. Takahashi, Y. Yang, A. Carréric, M. J. McPhaden, Increased variability of eastern Pacific El Niño under greenhouse warming. *Nature* **564**, 201–206 (2018). [doi:10.1038/s41586-018-0776-9](https://doi.org/10.1038/s41586-018-0776-9) Medline
10. W. Cai, B. Ng, G. Wang, A. Santoso, L. Wu, K. Yang, Increased ENSO sea surface temperature variability under four IPCC emission scenarios. *Nat. Clim. Chang.* **12**, 228–231 (2022). [doi:10.1038/s41558-022-01282-z](https://doi.org/10.1038/s41558-022-01282-z)
11. W. Cai, S. Borlace, M. Lengaigne, P. van Renssch, M. Collins, G. Vecchi, A. Timmermann, A. Santoso, M. J. McPhaden, L. Wu, M. H. England, G. Wang, E. Guilyardi, F.-F. Jin, Increasing frequency of extreme El Niño events due to greenhouse warming. *Nat. Clim. Chang.* **4**, 111–116 (2014). [doi:10.1038/nclimate2100](https://doi.org/10.1038/nclimate2100)
12. W. Cai, A. Santoso, M. Collins, B. Dewitte, C. Karamperidou, J.-S. Kug, M. Lengaigne, M. J. McPhaden, M. F. Stuecker, A. S. Taschetto, A. Timmermann, L. Wu, S.-W. Yeh, G. Wang, B. Ng, F. Jia, Y. Yang, J. Ying, X.-T. Zheng, T. Bayr, J. R. Brown, A. Capotondi, K. M. Cobb, B. Gan, T. Geng, Y.-G. Ham, F.-F. Jin, H.-S. Jo, X. Li, X. Lin, S. McGregor, J.-H. Park, K. Stein, K. Yang, L. Zhang, W. Zhong, Changing El Niño–Southern Oscillation in a warming climate. *Nat. Rev. Earth Environ.* **2**, 628–644 (2021). [doi:10.1038/s43017-021-00199-z](https://doi.org/10.1038/s43017-021-00199-z)
13. M. Burke, S. M. Hsiang, E. Miguel, Global non-linear effect of temperature on economic production. *Nature* **527**, 235–239 (2015). [doi:10.1038/nature15725](https://doi.org/10.1038/nature15725) Medline

14. M. Burke, V. Tanutama, “Climatic constraints on aggregate economic output” (NBER Working Paper 25779, National Bureau of Economic Research, 2019); <http://www.nber.org/papers/w25779>.
15. M. Dell, B. F. Jones, B. A. Olken, Temperature shocks and economic growth: Evidence from the last half century. *Am. Econ. J. Macroecon.* **4**, 66–95 (2012). [doi:10.1257/mac.4.3.66](https://doi.org/10.1257/mac.4.3.66)
16. M. Kalkuhl, L. Wenz, The impact of climate conditions on economic production. Evidence from a global panel of regions. *J. Environ. Econ. Manage.* **103**, 102360 (2020). [doi:10.1016/j.jeem.2020.102360](https://doi.org/10.1016/j.jeem.2020.102360)
17. M. Kotz, L. Wenz, A. Stechemesser, M. Kalkuhl, A. Levermann, Day-to-day temperature variability reduces economic growth. *Nat. Clim. Chang.* **11**, 319–325 (2021). [doi:10.1038/s41558-020-00985-5](https://doi.org/10.1038/s41558-020-00985-5)
18. P. Cashin, K. Mohaddes, M. Raissi, Fair weather or foul? The macroeconomic effects of El Niño. *J. Int. Econ.* **106**, 37–54 (2017). [doi:10.1016/j.inteco.2017.01.010](https://doi.org/10.1016/j.inteco.2017.01.010)
19. S. C. Smith, D. Ubilava, The El Niño Southern Oscillation and economic growth in the developing world. *Glob. Environ. Change* **45**, 151–164 (2017). [doi:10.1016/j.gloenvcha.2017.05.007](https://doi.org/10.1016/j.gloenvcha.2017.05.007)
20. R. Generoso, C. Couharde, O. Damette, K. Mohaddes, The growth effects of El Niño and La Niña: Local weather conditions matter. *Ann. Econ. Stat.* **140**, 83–126 (2020). [doi:10.15609/annaestat2009.140.0083](https://doi.org/10.15609/annaestat2009.140.0083)
21. A. D. Brunner, El Niño and world primary commodity prices: Warm water or hot air? *Rev. Econ. Stat.* **84**, 176–183 (2002). [doi:10.1162/003465302317332008](https://doi.org/10.1162/003465302317332008)
22. D. Ubilava, El Niño, La Niña, and world coffee price dynamics. *Agric. Econ.* **43**, 17–26 (2012). [doi:10.1111/j.1574-0862.2011.00562.x](https://doi.org/10.1111/j.1574-0862.2011.00562.x)
23. D. Ubilava, The ENSO effect and asymmetries in wheat price dynamics. *World Dev.* **96**, 490–502 (2017). [doi:10.1016/j.worlddev.2017.03.031](https://doi.org/10.1016/j.worlddev.2017.03.031)
24. F. C. Moore, D. B. Diaz, Temperature impacts on economic growth warrant stringent mitigation policy. *Nat. Clim. Chang.* **5**, 127–131 (2015). [doi:10.1038/nclimate2481](https://doi.org/10.1038/nclimate2481)
25. S. Dietz, N. Stern, Endogenous growth, convexity of damage and climate risk: How Nordhaus’ framework supports deep cuts in carbon emissions. *Econ. J. (London)* **125**, 574–620 (2015). [doi:10.1111/eco.12188](https://doi.org/10.1111/eco.12188)
26. E. J. Moyer, M. D. Woolley, N. J. Matteson, M. J. Glotter, D. A. Weisbach, Climate impacts on economic growth as drivers of uncertainty in the social cost of carbon. *J. Legal Stud.* **43**, 401–425 (2014). [doi:10.1086/678140](https://doi.org/10.1086/678140)
27. K. Takahashi, A. Montecinos, K. Goubanova, B. Dewitte, ENSO regimes: Reinterpreting the canonical and Modoki El Niño. *Geophys. Res. Lett.* **38**, L10704 (2011). [doi:10.1029/2011GL047364](https://doi.org/10.1029/2011GL047364)
28. E. M. Rasmusson, T. H. Carpenter, Variations in tropical sea surface temperature and surface wind fields associated with the Southern Oscillation/El Niño. *Mon. Weather Rev.* **110**, 354–384 (1982). [doi:10.1175/1520-0493\(1982\)110<0354:VITSST>2.0.CO;2](https://doi.org/10.1175/1520-0493(1982)110<0354:VITSST>2.0.CO;2)

29. D. Ubilava, M. Abdolrahimi, The El Niño impact on maize yields is amplified in lower income teleconnected countries. *Environ. Res. Lett.* **14**, 054008 (2019). [doi:10.1088/1748-9326/ab0cd0](https://doi.org/10.1088/1748-9326/ab0cd0)
30. S. Power, M. Haylock, R. Colman, X. Wang, The predictability of interdecadal changes in ENSO activity and ENSO teleconnections. *J. Clim.* **19**, 4755–4771 (2006). [doi:10.1175/JCLI3868.1](https://doi.org/10.1175/JCLI3868.1)
31. B. A. Bastien-Olvera, F. Granella, F. C. Moore, Persistent effect of temperature on GDP identified from lower frequency temperature variability. *Environ. Res. Lett.* **17**, 084038 (2022). [doi:10.1088/1748-9326/ac82c2](https://doi.org/10.1088/1748-9326/ac82c2)
32. M. Kotz, A. Levermann, L. Wenz, The effect of rainfall changes on economic production. *Nature* **601**, 223–227 (2022). [doi:10.1038/s41586-021-04283-8](https://doi.org/10.1038/s41586-021-04283-8) [Medline](#)
33. N. S. Diffenbaugh, F. V. Davenport, M. Burke, Historical warming has increased U.S. crop insurance losses. *Environ. Res. Lett.* **16**, 084025 (2021). [doi:10.1088/1748-9326/ac1223](https://doi.org/10.1088/1748-9326/ac1223)
34. W. Cai, G. Wang, A. Santoso, M. J. McPhaden, L. Wu, F.-F. Jin, A. Timmermann, M. Collins, G. Vecchi, M. Lengaigne, M. H. England, D. Dommenget, K. Takahashi, E. Guilyardi, Increased frequency of extreme La Niña events under greenhouse warming. *Nat. Clim. Chang.* **5**, 132–137 (2015). [doi:10.1038/nclimate2492](https://doi.org/10.1038/nclimate2492)
35. M. K. van Aalst, S. Fankhauser, S. M. Kane, K. Sponberg, “Climate information and forecasting for development: lessons from the 1997/98 El Niño” (Environment Department Paper No. 79, Climate Change Series, World Bank Group, 2000); <http://documents.worldbank.org/curated/en/451971468739263265/Climate-information-and-forecasting-for-development-lessons-from-the-1997-98-El-Nino>.
36. W. Cai, B. Ng, T. Geng, L. Wu, A. Santoso, M. J. McPhaden, Butterfly effect and a self-modulating El Niño response to global warming. *Nature* **585**, 68–73 (2020). [doi:10.1038/s41586-020-2641-x](https://doi.org/10.1038/s41586-020-2641-x) [Medline](#)
37. N. Maher, D. Matei, S. Milinski, J. Marotzke, ENSO change in climate projections: Forced response or internal variability? *Geophys. Res. Lett.* **45**, 11390–11398 (2018). [doi:10.1029/2018GL079764](https://doi.org/10.1029/2018GL079764)
38. C. Deser, R. Knutti, S. Solomon, A. S. Phillips, Communication of the role of natural variability in future North American climate. *Nat. Clim. Chang.* **2**, 775–779 (2012). [doi:10.1038/nclimate1562](https://doi.org/10.1038/nclimate1562)
39. K.-S. Yun, J.-Y. Lee, A. Timmermann, K. Stein, M. F. Stuecker, J. C. Fyfe, E.-S. Chung, Increasing ENSO–rainfall variability due to changes in future tropical temperature–rainfall relationship. *Commun. Earth Environ.* **2**, 43 (2021). [doi:10.1038/s43247-021-00108-8](https://doi.org/10.1038/s43247-021-00108-8)
40. K. Hu, G. Huang, P. Huang, Y. Kosaka, S.-P. Xie, Intensification of El Niño-induced atmospheric anomalies under greenhouse warming. *Nat. Geosci.* **14**, 377–382 (2021). [doi:10.1038/s41561-021-00730-3](https://doi.org/10.1038/s41561-021-00730-3)
41. A. T. Wittenberg, A. Rosati, T. L. Delworth, G. A. Vecchi, F. Zeng, ENSO modulation: Is it decadally predictable? *J. Clim.* **27**, 2667–2681 (2014). [doi:10.1175/JCLI-D-13-00577.1](https://doi.org/10.1175/JCLI-D-13-00577.1)

42. C. W. Callahan, C. Chen, M. Rugenstein, J. Bloch-Johnson, S. Yang, E. J. Moyer, Robust decrease in El Niño/Southern Oscillation amplitude under long-term warming. *Nat. Clim. Chang.* **11**, 752–757 (2021). [doi:10.1038/s41558-021-01099-2](https://doi.org/10.1038/s41558-021-01099-2)
43. Council of Economic Advisers, “Discounting for public policy: Theory and recent evidence on the merits of updating the discount rate,” Issue Brief, January 2017; https://obamawhitehouse.archives.gov/sites/default/files/page/files/201701_cea_discounting_issue_brief.pdf.
44. M. Meinshausen, J. Lewis, C. McGlade, J. Gütschow, Z. Nicholls, R. Burdon, L. Cozzi, B. Hackmann, Realization of Paris Agreement pledges may limit warming just below 2 °C. *Nature* **604**, 304–309 (2022). [doi:10.1038/s41586-022-04553-z](https://doi.org/10.1038/s41586-022-04553-z) Medline
45. M. Davis, *Late Victorian Holocausts: El Niño Famines and the Making of the Third World* (Verso Books, 2002).
46. C. W. Callahan, J. S. Mankin, Globally unequal effect of extreme heat on economic growth. *Sci. Adv.* **8**, eadd3726 (2022). [doi:10.1126/sciadv.add3726](https://doi.org/10.1126/sciadv.add3726) Medline
47. B. O’Neill, M. van Aalst, Z. Zaiton Ibrahim, L. Berrang Ford, S. Bhadwal, H. Buhaug, D. Diaz, K. Frieler, M. Garschagen, A. Magnan, G. Midgely, A. Mirzabaev, A. Thomas, R. Warren, “Key risks across sectors and regions” in *Climate Change 2022: Impacts, Adaptation and Vulnerability. Contribution of Working Group II to the Sixth Assessment Report of the Intergovernmental Panel on Climate Change* (Cambridge Univ. Press, USA, 2022), pp. 2411–2538.
48. A. French, R. Mechler, “Managing El Niño risks under uncertainty in Peru” (International Institute for Applied Systems Analysis, 2017); https://pure.iiasa.ac.at/id/eprint/14849/1/French_Mechler_2017_El%20Ni%C3%b1o_Risk_Peru_Report.pdf.
49. N. A. Rayner, D. E. Parker, E. B. Horton, C. K. Folland, L. V. Alexander, D. P. Rowell, E. C. Kent, A. Kaplan, Global analyses of sea surface temperature, sea ice, and night marine air temperature since the late nineteenth century. *J. Geophys. Res.* **108**, 4407 (2003). [doi:10.1029/2002JD002670](https://doi.org/10.1029/2002JD002670)
50. R. A. Rohde, Z. Hausfather, The Berkeley Earth Land/Ocean Temperature Record. *Earth Syst. Sci. Data* **12**, 3469–3479 (2020). [doi:10.5194/essd-12-3469-2020](https://doi.org/10.5194/essd-12-3469-2020)
51. U. Schneider, A. Becker, P. Finger, A. Meyer-Christoffer, B. Rudolf, M. Ziese, GPCC full data reanalysis version 6.0 at 0.5°: monthly land-surface precipitation from rain-gauges built on GTS-based and historic data, Global Precipitation Climatology Centre (2011); http://dx.doi.org/10.5676/DWD_GPCC/FD_M_V6_050.
52. Center for International Earth Science Information Network (CIESIN), Columbia University, Gridded Population of the World, Version 4 (GPWv4): Population Count (NASA Socioeconomic Data and Applications Center, 2016); <http://dx.doi.org/10.7927/H4X63JVC>.
53. R. C. Feenstra, R. Inklaar, M. P. Timmer, The next generation of the Penn World Table. *Am. Econ. Rev.* **105**, 3150–3182 (2015). [doi:10.1257/aer.20130954](https://doi.org/10.1257/aer.20130954)

54. A. Deaton, A. Heston, Understanding PPPs and PPP-based national accounts. *Am. Econ. J. Macroecon.* **2**, 1–35 (2010). [doi:10.1257/mac.2.4.1](https://doi.org/10.1257/mac.2.4.1)
55. The World Bank, *World Development Indicators 2016* (World Bank, 2016).
56. V. Eyring, S. Bony, G. A. Meehl, C. A. Senior, B. Stevens, R. J. Stouffer, K. E. Taylor, Overview of the Coupled Model Intercomparison Project Phase 6 (CMIP6) experimental design and organization. *Geosci. Model Dev.* **9**, 1937–1958 (2016). [doi:10.5194/gmd-9-1937-2016](https://doi.org/10.5194/gmd-9-1937-2016)
57. B. C. O'Neill, C. Tebaldi, D. P. van Vuuren, V. Eyring, P. Friedlingstein, G. Hurtt, R. Knutti, E. Kriegler, J.-F. Lamarque, J. Lowe, G. A. Meehl, R. Moss, K. Riahi, B. M. Sanderson, The Scenario Model Intercomparison Project (ScenarioMIP) for CMIP6. *Geosci. Model Dev.* **9**, 3461–3482 (2016). [doi:10.5194/gmd-9-3461-2016](https://doi.org/10.5194/gmd-9-3461-2016)
58. C. Tebaldi, K. Debeire, V. Eyring, E. Fischer, J. Fyfe, P. Friedlingstein, R. Knutti, J. Lowe, B. O'Neill, B. Sanderson, D. van Vuuren, K. Riahi, M. Meinshausen, Z. Nicholls, K. B. Tokarska, G. Hurtt, E. Kriegler, J.-F. Lamarque, G. Meehl, R. Moss, S. E. Bauer, O. Boucher, V. Brovkin, Y.-H. Byun, M. Dix, S. Gualdi, H. Guo, J. G. John, S. Kharin, Y. Kim, T. Koshiro, L. Ma, D. Olivié, S. Panickal, F. Qiao, X. Rong, N. Rosenbloom, M. Schupfner, R. Séférian, A. Sellar, T. Semmler, X. Shi, Z. Song, C. Steger, R. Stouffer, N. Swart, K. Tachiiri, Q. Tang, H. Tatebe, A. Voldoire, E. Volodin, K. Wyser, X. Xin, S. Yang, Y. Yu, T. Ziehn, Climate model projections from the Scenario Model Intercomparison Project (ScenarioMIP) of CMIP6. *Earth Syst. Dyn.* **12**, 253–293 (2021). [doi:10.5194/esd-12-253-2021](https://doi.org/10.5194/esd-12-253-2021)
59. S. Hoyer, J. Hamman, xarray: N-D labeled arrays and datasets in Python. *J. Open Res. Softw.* **5**, 10 (2017). [doi:10.5334/jors.148](https://doi.org/10.5334/jors.148)
60. F. Jia, W. Cai, B. Gan, L. Wu, E. Di Lorenzo, Enhanced North Pacific impact on El Niño/Southern Oscillation under greenhouse warming. *Nat. Clim. Chang.* **11**, 840–847 (2021). [doi:10.1038/s41558-021-01139-x](https://doi.org/10.1038/s41558-021-01139-x)
61. B. Ng, W. Cai, T. Cowan, D. Bi, Impacts of low-frequency internal climate variability and greenhouse warming on El Niño–Southern Oscillation. *J. Clim.* **34**, 2205–2218 (2021). [doi:10.1175/JCLI-D-20-0232.1](https://doi.org/10.1175/JCLI-D-20-0232.1)
62. E. Tziperman, M. A. Cane, S. E. Zebiak, Y. Xue, B. Blumenthal, Locking of El Niño’s peak time to the end of the calendar year in the delayed oscillator picture of ENSO. *J. Clim.* **11**, 2191–2199 (1998). [doi:10.1175/1520-0442\(1998\)011<2191:LOENOS>2.0.CO;2](https://doi.org/10.1175/1520-0442(1998)011<2191:LOENOS>2.0.CO;2)
63. M. Newman, P. D. Sardeshmukh, Are we near the predictability limit of tropical Indo-Pacific sea surface temperatures? *Geophys. Res. Lett.* **44**, 8520–8529 (2017). [doi:10.1002/2017GL074088](https://doi.org/10.1002/2017GL074088)
64. C. D. Kolstad, F. C. Moore, Estimating the economic impacts of climate change using weather observations. *Rev. Environ. Econ. Policy* **14**, 1–24 (2020). [doi:10.1093/reep/rez024](https://doi.org/10.1093/reep/rez024)
65. M. Burke, W. M. Davis, N. S. Diffenbaugh, Large potential reduction in economic damages under UN mitigation targets. *Nature* **557**, 549–553 (2018). [doi:10.1038/s41586-018-0071-9](https://doi.org/10.1038/s41586-018-0071-9) [Medline](#)

66. S. M. Hsiang, A. S. Jina, “The causal effect of environmental catastrophe on long-run economic growth: Evidence from 6,700 cyclones” (NBER Working Paper 20352, National Bureau of Economic Research, 2014); <http://www.nber.org/papers/w20352>.
67. S. Hsiang, Climate econometrics. *Annu. Rev. Resour. Econ.* **8**, 43–75 (2016).
[doi:10.1146/annurev-resource-100815-095343](https://doi.org/10.1146/annurev-resource-100815-095343)
68. J. H. Stock, M. W. Watson, Vector autoregressions. *J. Econ. Perspect.* **15**, 101–115 (2001).
[doi:10.1257/jep.15.4.101](https://doi.org/10.1257/jep.15.4.101)
69. N. S. Diffenbaugh, M. Burke, Global warming has increased global economic inequality. *Proc. Natl. Acad. Sci. U.S.A.* **116**, 9808–9813 (2019). [doi:10.1073/pnas.1816020116](https://doi.org/10.1073/pnas.1816020116)
[Medline](#)
70. E. Guilyardi, A. Wittenberg, A. Fedorov, M. Collins, C. Wang, A. Capotondi, G. J. van Oldenborgh, T. Stockdale, Understanding El Niño in ocean–atmosphere general circulation models: Progress and challenges. *Bull. Am. Meteorol. Soc.* **90**, 325–340 (2009). [doi:10.1175/2008BAMS2387.1](https://doi.org/10.1175/2008BAMS2387.1)
71. R. Seager, M. Cane, N. Henderson, D.-E. Lee, R. Abernathey, H. Zhang, Strengthening tropical Pacific zonal sea surface temperature gradient consistent with rising greenhouse gases. *Nat. Clim. Chang.* **9**, 517–522 (2019). [doi:10.1038/s41558-019-0505-x](https://doi.org/10.1038/s41558-019-0505-x)
72. C. Karamperidou, F.-F. Jin, J. L. Conroy, The importance of ENSO nonlinearities in tropical pacific response to external forcing. *Clim. Dyn.* **49**, 2695–2704 (2017).
[doi:10.1007/s00382-016-3475-y](https://doi.org/10.1007/s00382-016-3475-y)
73. A. C. Baker, D. F. Larcker, C. C. Y. Wang, How much should we trust staggered difference-in-differences estimates? *J. Financ. Econ.* **144**, 370–395 (2022).
[doi:10.1016/j.jfineco.2022.01.004](https://doi.org/10.1016/j.jfineco.2022.01.004)
74. C. de Chaisemartin, X. D'Haultfoeuille, “Two-way fixed effects and differences-in-differences with heterogeneous treatment effects: A survey” (NBER Working Paper 29691, National Bureau of Economic Research, 2022);
<http://www.nber.org/papers/w29691>.
75. J. Roth, P. H. C. Sant'Anna, A. Bilinski, J. Poe, What's trending in difference-in-differences? A synthesis of the recent econometrics literature. [arXiv:2201.01194](https://arxiv.org/abs/2201.01194) [econ.EM] (2023).
76. B. Callaway, P. H. C. Sant'Anna, Difference-in-differences with multiple time periods. *J. Econom.* **225**, 200–230 (2021). [doi:10.1016/j.jeconom.2020.12.001](https://doi.org/10.1016/j.jeconom.2020.12.001)
77. B. Callaway, A. Goodman-Bacon, P. H. C. Sant'Anna, Difference-in-differences with a continuous treatment. [arXiv:2107.02637](https://arxiv.org/abs/2107.02637) [econ.EM] (2021).
78. C. de Chaisemartin, X. D'Haultfœuille, Two-way fixed effects estimators with heterogeneous treatment effects. *Am. Econ. Rev.* **110**, 2964–2996 (2020). [doi:10.1257/aer.20181169](https://doi.org/10.1257/aer.20181169)
79. C. de Chaisemartin, X. D'Haultfœuille, F. Pasquier, G. Vazquez-Bare, Difference-in-differences estimators for treatments continuously distributed at every period. [arXiv:2201.06898](https://arxiv.org/abs/2201.06898) [econ.EM] (2022).
80. P. Jakielka, Simple diagnostics for two-way fixed effects. [arXiv:2103.13229](https://arxiv.org/abs/2103.13229) [econ.GN] (2021).

81. R. Knutti, J. Sedláček, B. M. Sanderson, R. Lorenz, E. M. Fischer, V. Eyring, A climate model projection weighting scheme accounting for performance and interdependence. *Geophys. Res. Lett.* **44**, 1909–1918 (2017). [doi:10.1002/2016GL072012](https://doi.org/10.1002/2016GL072012)
82. R. Knutti, The end of model democracy? *Clim. Change* **102**, 395–404 (2010). [doi:10.1007/s10584-010-9800-2](https://doi.org/10.1007/s10584-010-9800-2)
83. P. Huang, J. Ying, A multimodel ensemble pattern regression method to correct the tropical Pacific SST change patterns under global warming. *J. Clim.* **28**, 4706–4723 (2015). [doi:10.1175/JCLI-D-14-00833.1](https://doi.org/10.1175/JCLI-D-14-00833.1)
84. D. Chen, M. A. Cane, S. E. Zebiak, R. Cañizares, A. Kaplan, Bias correction of an ocean-atmosphere coupled model. *Geophys. Res. Lett.* **27**, 2585–2588 (2000). [doi:10.1029/1999GL011078](https://doi.org/10.1029/1999GL011078)

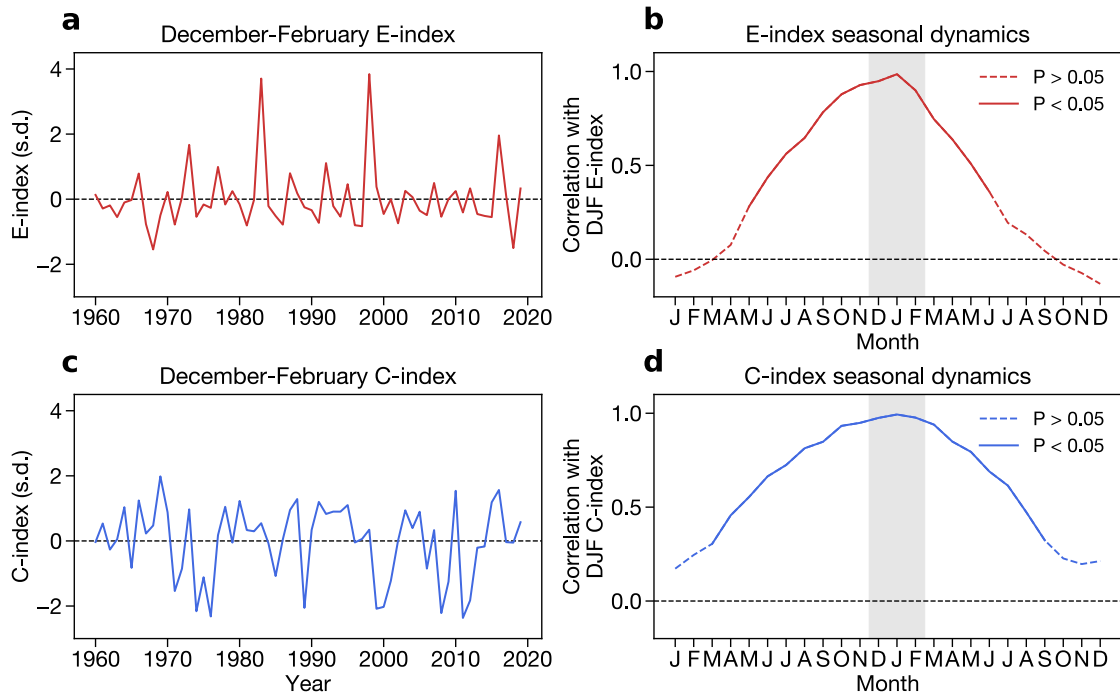


Fig. S1.

Interannual and seasonal dynamics of the E- and C-index. A) Timeseries of the average E-index over December, January, and February (DJF) of each year, where the values are referenced to the year of January and February. B) Pearson correlation coefficient between the E-index in each month and the DJF-mean E-index. Solid lines denote correlation coefficients that are statistically significant ($p < 0.05$) and dashed lines denote correlation coefficients that are statistically insignificant ($p > 0.05$). C) As in (A), but for the DJF C-index. D) As in (B), but for the DJF C-index.

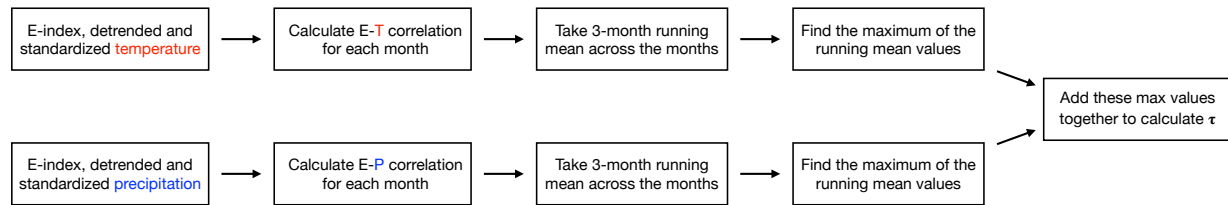


Fig. S2

Flow chart for calculation of country-level E-index teleconnections. An analogous calculation is made for C-index teleconnections.

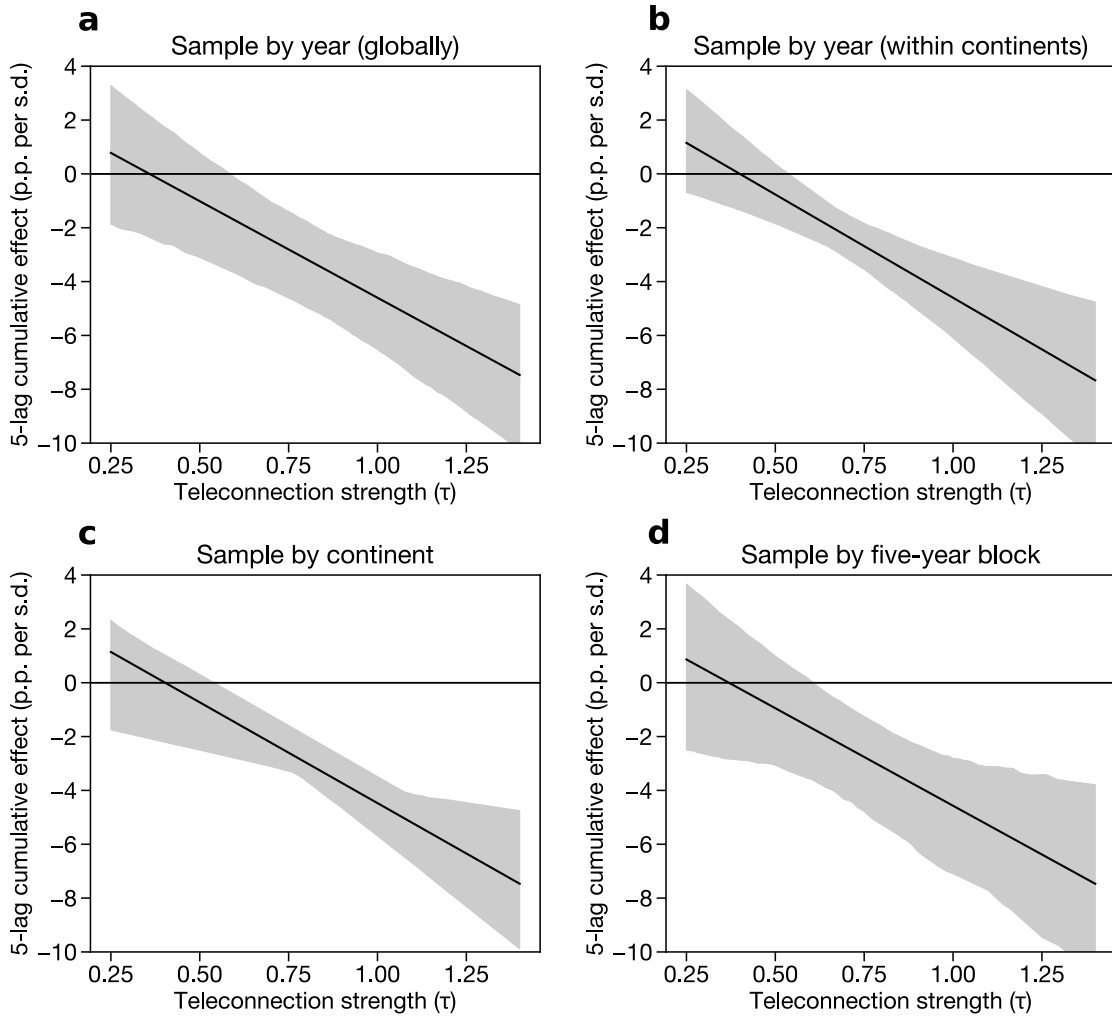


Fig. S3

Regression results using alternative bootstrap sampling schemes. A) Cumulative 5-lag effect of ENSO on economic growth when sampling by year, keeping all countries from a given year together, to account for global spatial correlation in growth within a given year. B) Effect when sampling by continent-year combinations to account for spatial correlation in growth within specific continents in a given year. C) Effect when sampling by continents to account for simultaneous within-continent temporal and spatial correlation in growth. D) Effect when sampling by five-year blocks to account for global spatial correlation in growth and short-term (i.e., five-year) temporal correlation in growth. In all cases, solid line shows the mean and shading shows the 95% confidence intervals. All samples are taken from uniform distributions with replacement. All axes are the same ranges across panels.

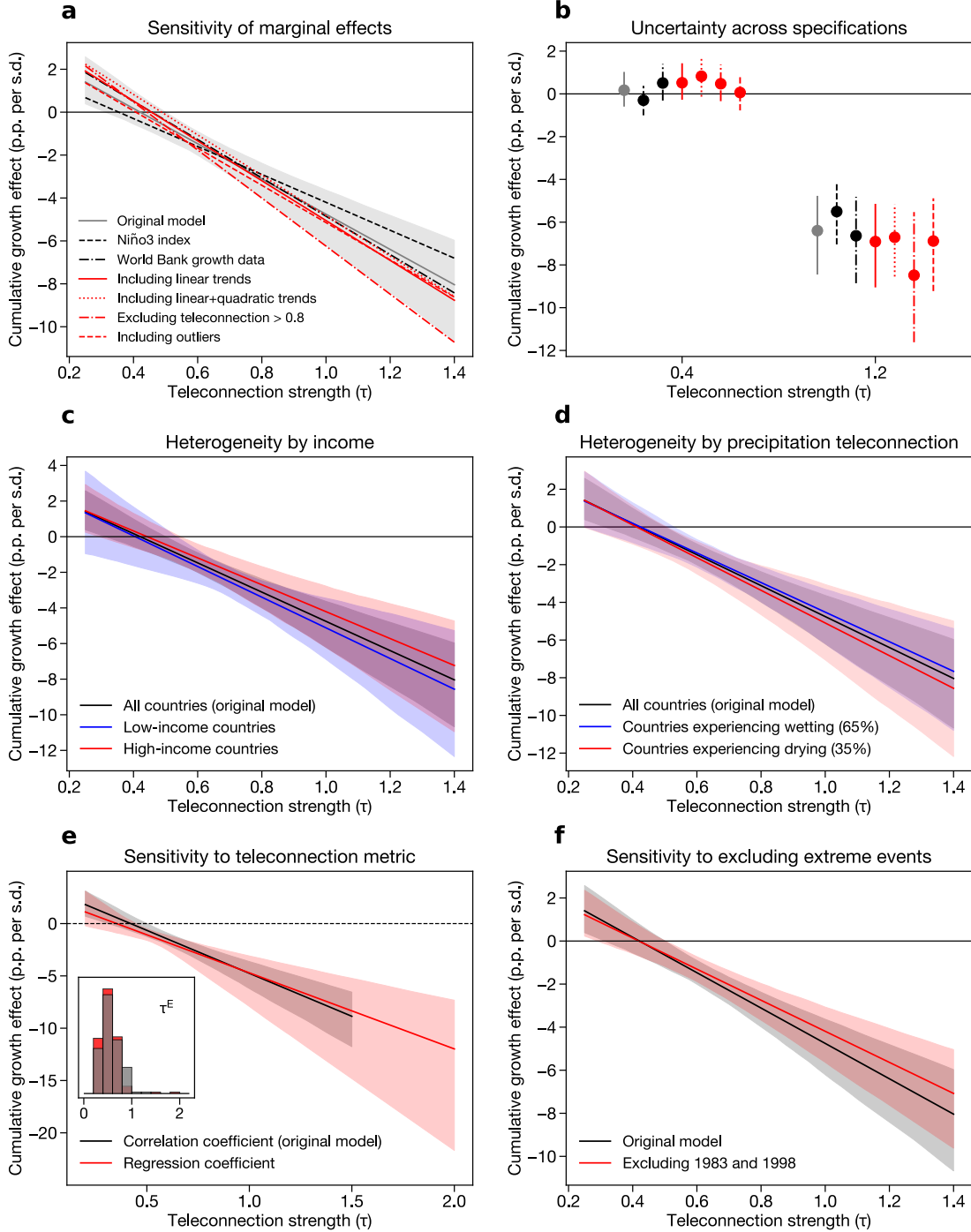


Fig. S4

Sensitivity and heterogeneity of the effect of El Niño. A) Cumulative 5-lag effect of El Niño on growth across a range of specifications: the main model (gray line shows mean and shading shows 95% confidence intervals), a model using the Niño3 index instead of the E- and C-index (black dashed line), a model using World Bank growth data instead of the Penn World Tables (black dash-dot line), a model that includes a country-specific linear trend in growth (red solid line), a model that includes both linear and quadratic country-specific trends (red dotted line), a

model that excludes countries with teleconnection values greater than 0.8 (red dash-dot line), and a model that includes outliers with absolute values of growth greater than 18% (red dashed line). B) Uncertainty in the 5-year cumulative marginal effects of El Niño across each model specification at two representative teleconnection values (0.4 and 1.2). Line styles denote alternative models presented in (A). C) Cumulative marginal effects of El Niño for low-income countries (blue) and high-income countries (red), as defined by World Bank income classifications (Methods). D) Cumulative marginal effects of El Niño for countries experiencing wetting in response to El Niño (positive correlation between the E-index and precipitation, blue) and countries experiencing drying (negative correlation between the E-index and precipitation, red). For each of these samples, we use the original teleconnection value calculated with absolute values in the distributed lag model, but split the sample by the sign of the precipitation teleconnection. In (C) and (D), the original model estimated for all countries is shown in black. E) Cumulative marginal effects of El Niño when using the partial correlation coefficient to measure teleconnections (the main analysis) and when using the regression coefficient instead (red). Inset histograms show the distribution of the two teleconnection metrics. F) Cumulative marginal effects of El Niño when using the full sample (the main analysis, black) and when dropping 1983 and 1998 from the sample (red). In panels (C), (D), (E), and (F), solid line denotes the average and shading denotes 95% confidence intervals from bootstrap resampling by country (Methods).

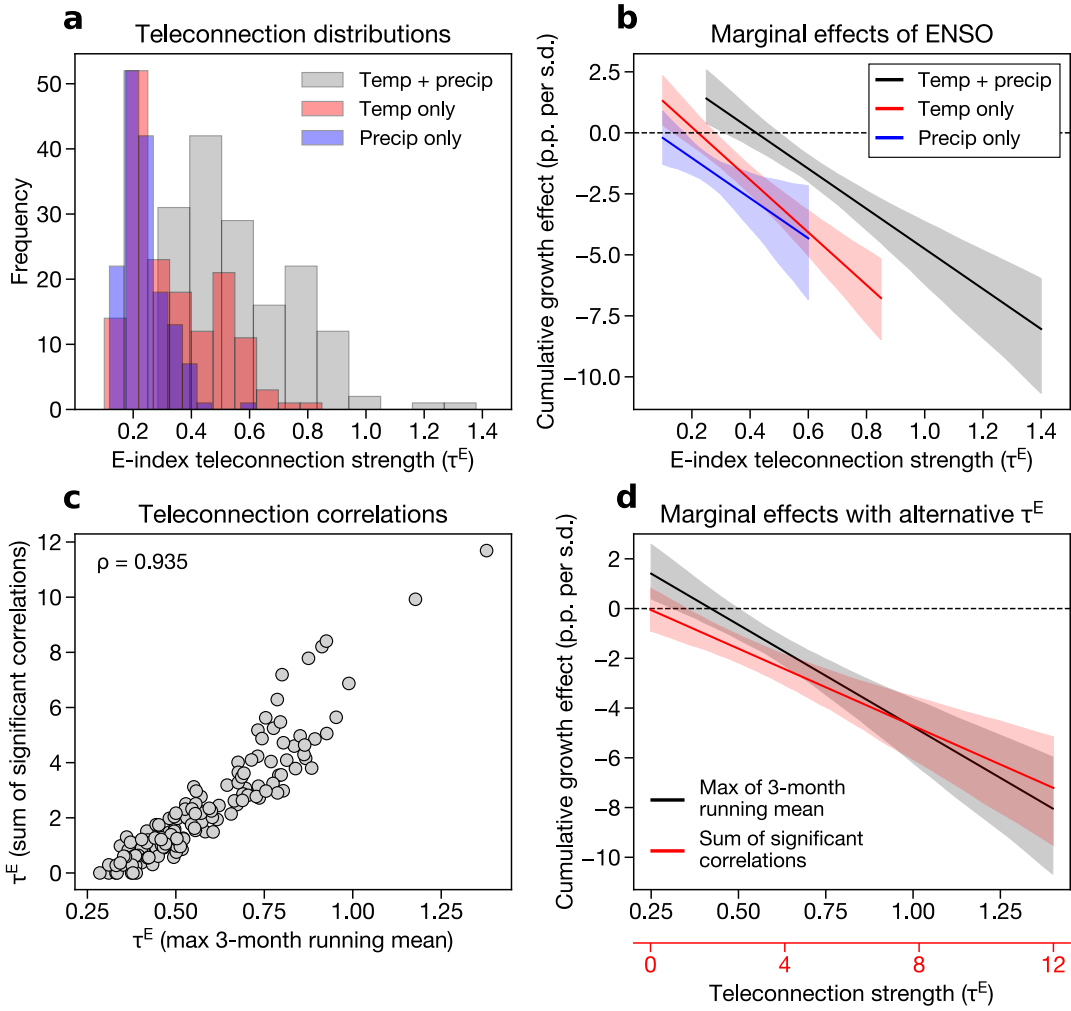


Fig. S5

Comparison of results using alternative teleconnection metrics. A) Distributions of country-level teleconnections using monthly temperature correlation coefficients (red), monthly precipitation correlation coefficients (blue), and their sum (gray). All values are positive since we transform the correlations to absolute values. B) Cumulative 5-lag effect of ENSO on economic growth using temperature-only teleconnections (red), precipitation-only teleconnections (blue), and temperature-plus-precipitation teleconnections (black). C) Relationship between teleconnections from our main analysis (maximum of three-month running mean) and alternative teleconnections using the sum of all statistically significant correlation coefficients across the months for each country. Rho denotes the Spearman's rank correlation coefficient between the two teleconnection metrics. D) Cumulative 5-lag effect of ENSO on economic growth using the original metric (black) and the summed correlation coefficient teleconnection metric (red). In (B) and (D), solid line shows mean and shading shows 95% confidence intervals across 1000 bootstrap iterations, as in the main analysis.

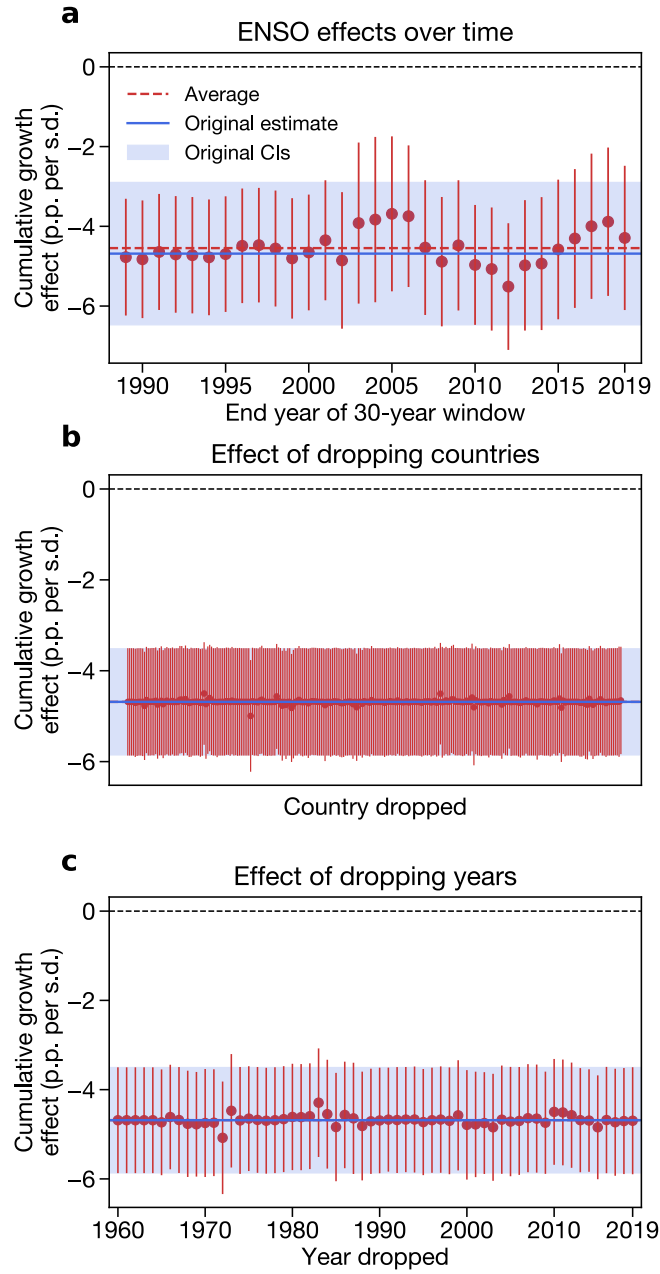


Fig. S6

Treatment effect heterogeneity. Panel (A) shows the effect of ENSO on countries with $\tau = 1.0$ calculated in thirty-year rolling windows. X-axis tick refers to the last year of the window. Panel (B) shows the effect of ENSO on countries with $\tau = 1.0$ when individual countries are dropped from the sample. We omit country labels for simplicity. Panel (C) shows the effect of ENSO on countries with $\tau = 1.0$ when individual years are dropped from the sample. In all panels, dashed red line shows the average effect from all the subsamples, solid blue line shows the central estimate from our original model, and blue shading shows the 95% confidence interval from our original model.

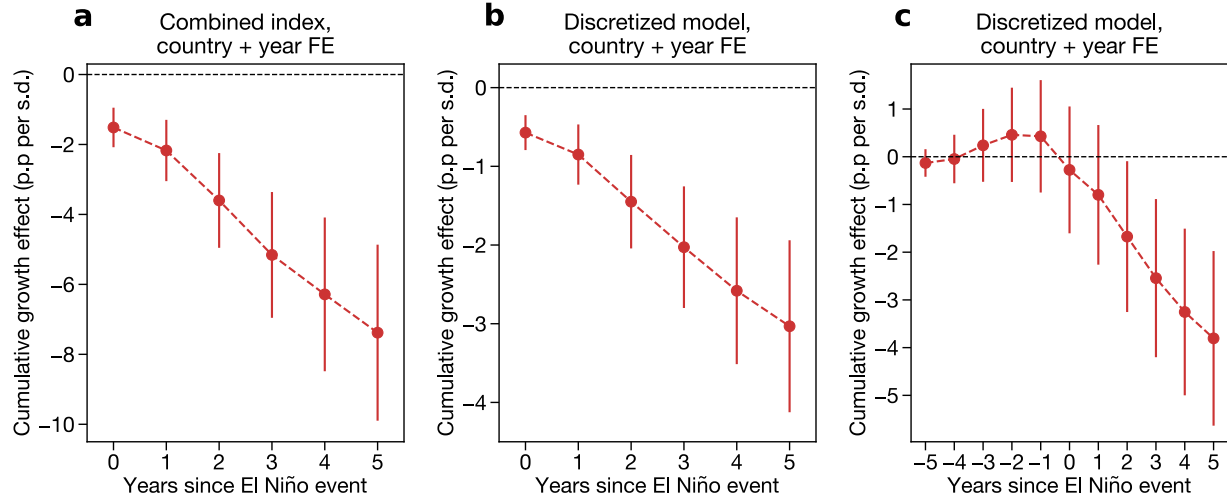


Fig. S7

Regression results using several alternative models with both country and year fixed effects. Panel (A) shows the cumulative effect of a 1-unit increase in the combined index resulting from multiplying E and τ^E . This index varies in both space and time simultaneously, meaning that both country and year fixed effects can be included. Panel (B) shows the average cumulative effect of a 1-s.d. increase in E across all “treated” countries, where treated countries are defined as those with $\tau^E > 0.5$. Panel (C) shows the same result as (B), with five leads of the E -index added along with lags. In all cases, the central dashed line shows the mean marginal effect and vertical bars show the 95% confidence intervals from bootstrap resampling by country.

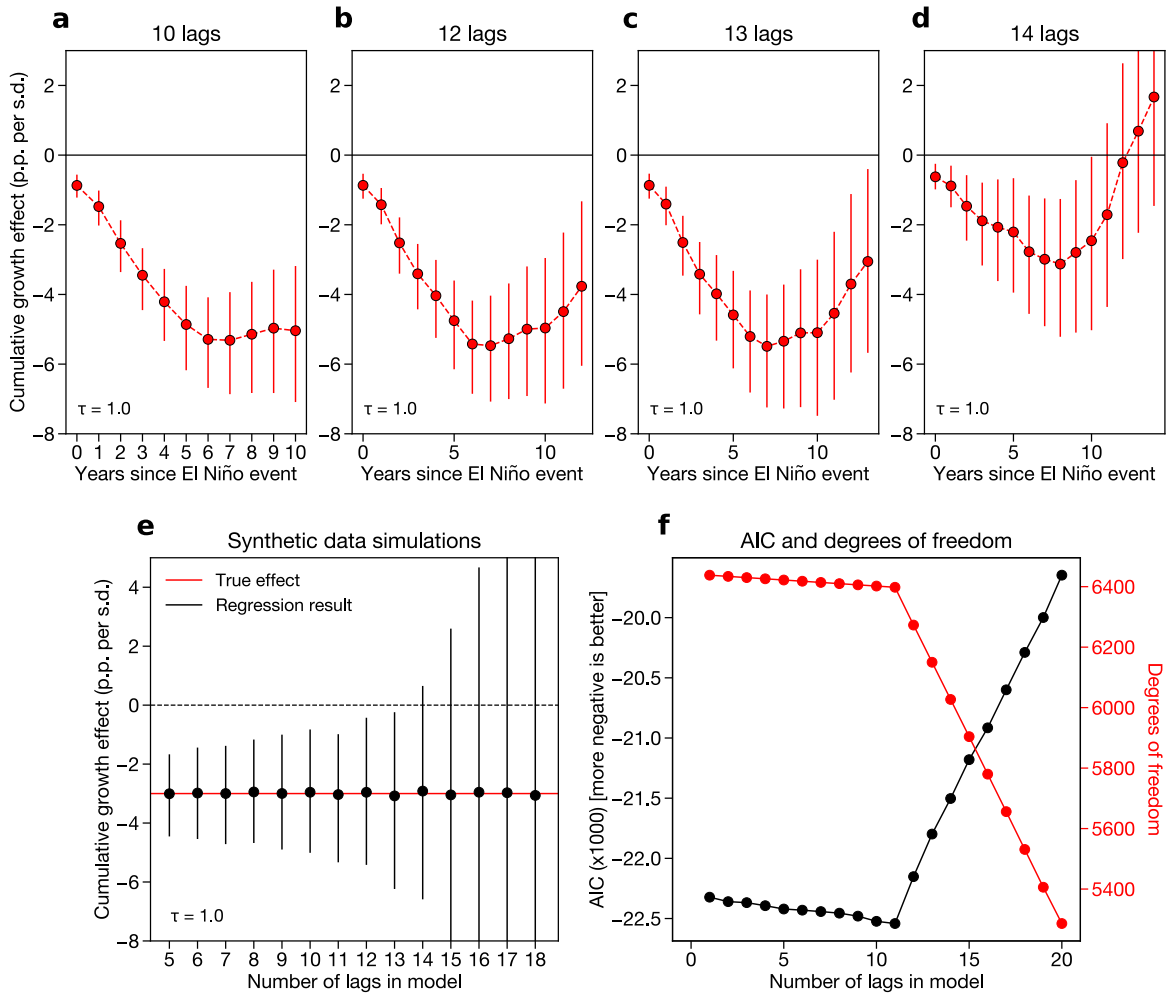


Fig. S8

Sensitivity of main regression results to additional lags. A-D) Regression results for countries with teleconnections greater than or equal to 1.0, estimated with 10 (A), 12 (B), 13 (C), or 14 (D) lags in the regression model. Confidence intervals are estimated by bootstrap resampling as in the main analysis. E) Results from synthetic data simulations where a “true” negative ENSO growth effect is imputed to the data and then estimated using models with lags between 5 and 18 (Methods). Coefficients estimated using this perfect model framework are shown for a hypothetical country with $\tau = 1.0$. F) Black line shows Akaike Information Criterion (AIC) values for a series of regression models with an increasing number of lags from 1 to 20. More negative AIC values are more desirable. AIC values are divided by 1000 for readability. Red line shows the number of degrees of freedom for the same set of models.

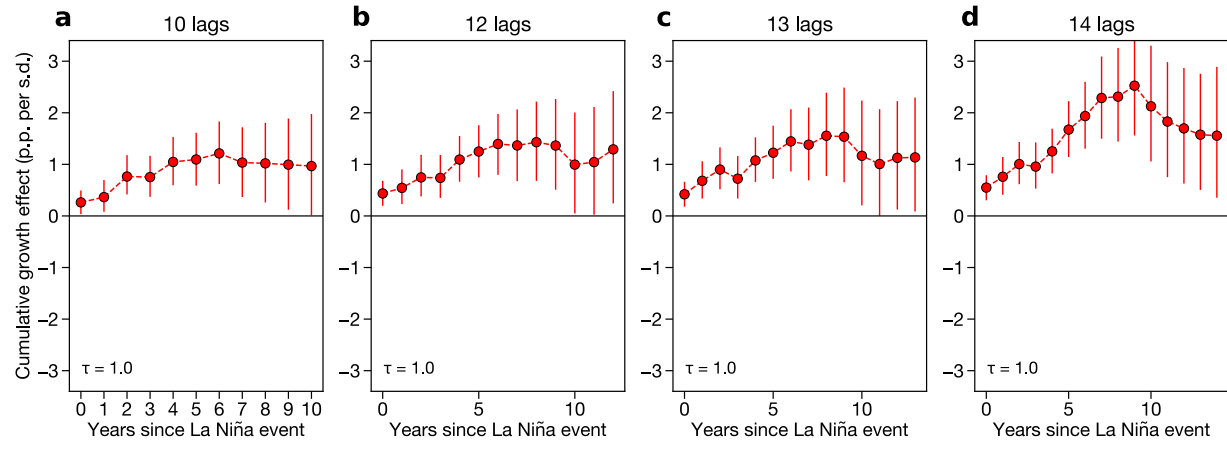


Fig. S9

Sensitivity of C-index regression results to additional lags. As in Fig. S7a-d, but for the C-index coefficients. The sign on the coefficients is flipped to measure the effect of moving from 0 to -1 (i.e., moving a neutral state to a La Niña state).

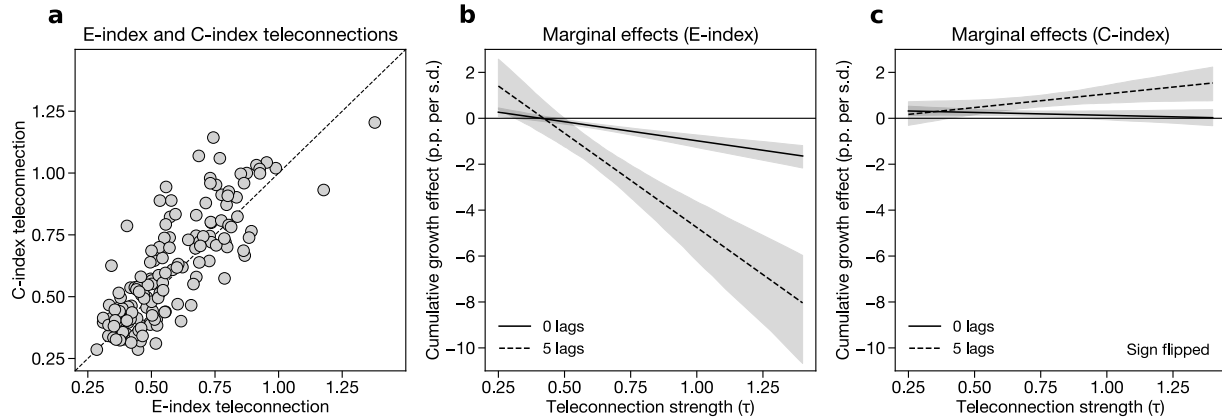


Fig. S10

Teleconnections and marginal effects for both the E-index and C-index. A) Comparison of country-specific teleconnection metrics calculated using the E-index (x-axis) and C-index (y-axis). Dashed line denotes the one-to-one line. B) Marginal effects of El Niño (measured by the E-index) at 0 and 5 lags across a range of teleconnection values. C) Marginal effects of La Niña (measured by the C-index) at 0 and 5 lags across a range of teleconnection values. The sign on the coefficients in (C) is flipped to measure the effect of moving from 0 to -1 (i.e., moving from a neutral state to a La Niña state). In (B) and (C), effects are calculated from a regression that includes both the E-index and C-index and their corresponding teleconnection metrics (Methods). Lines denote averages and shading denotes 95% confidence intervals using bootstrap resampling by country (Methods).

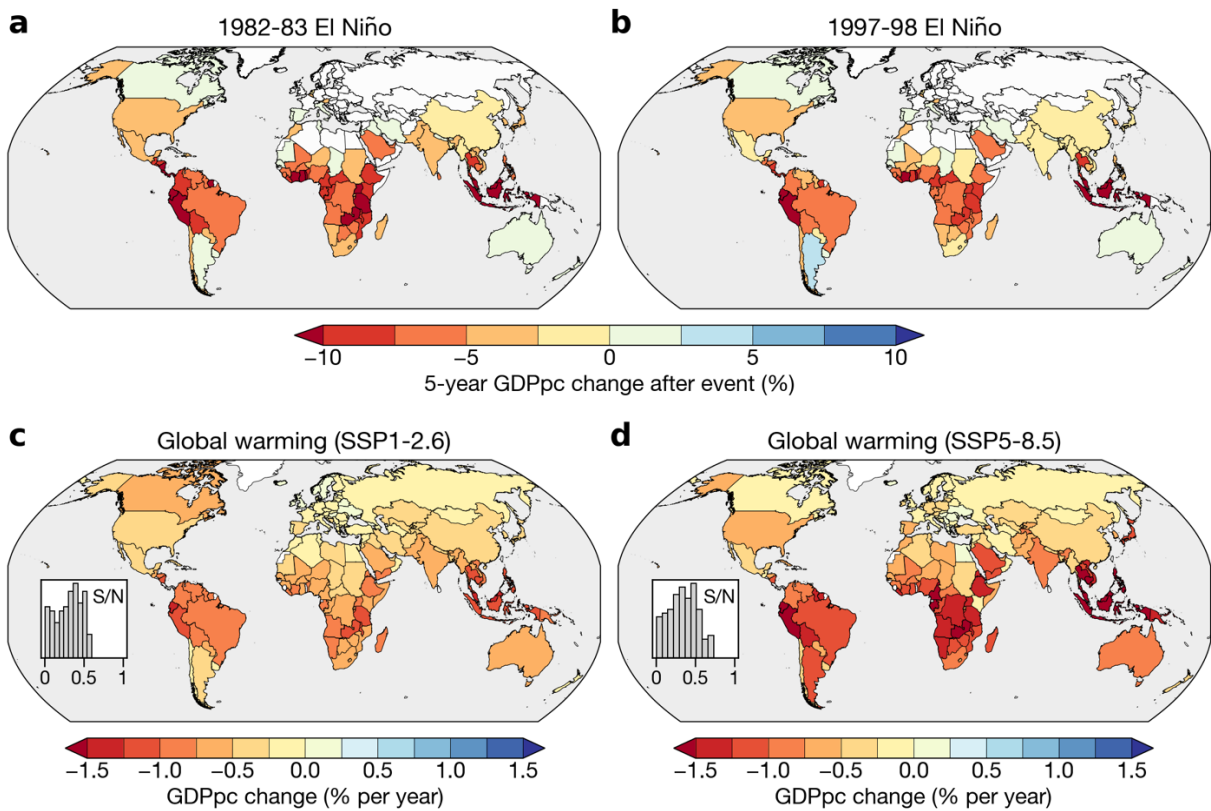


Fig. S11

Country-level losses from extreme El Niño events and global warming. A, B) Change in country-level GDPpc five years after two specific extreme El Niño events: 1982-83 (A) and 1997-98 (B). Changes are calculated relative to counterfactual trajectories in which the event did not occur (see Fig. 2a for example of Peru). That is, the color for Brazil in panel B indicates that Brazil's GDP per capita would have been 5% larger in 2003 if the 1997-98 El Niño event did not occur. Countries are masked in white if they either have no significant marginal effect of ENSO or do not have continuous GDPpc data since 1982 (Methods). C, D) 2020-2099 average change in country-level GDPpc under the SSP1-2.6 (C) and SSP5-8.5 (D) scenarios for the average case across climate models and regression bootstraps. Insets in C and D show the signal-to-noise ratios (S/N), meaning the absolute value of the ratio of the ensemble mean GDPpc change to the ensemble standard deviation GDPpc change. “Ensemble” is defined as all possible combinations of climate model projections and regression bootstraps.

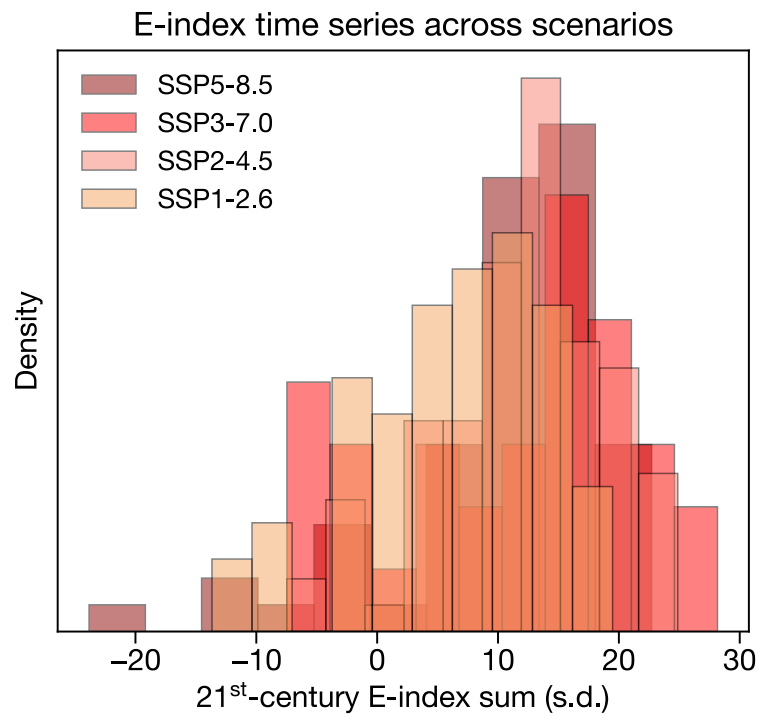


Fig. S12

E-index sum across scenarios. Histograms show the distribution of 2020-99 E-index sum values across simulations within each SSP scenario. Positive values mean that the simulation's E-index time series has more El Niños than La Niñas.

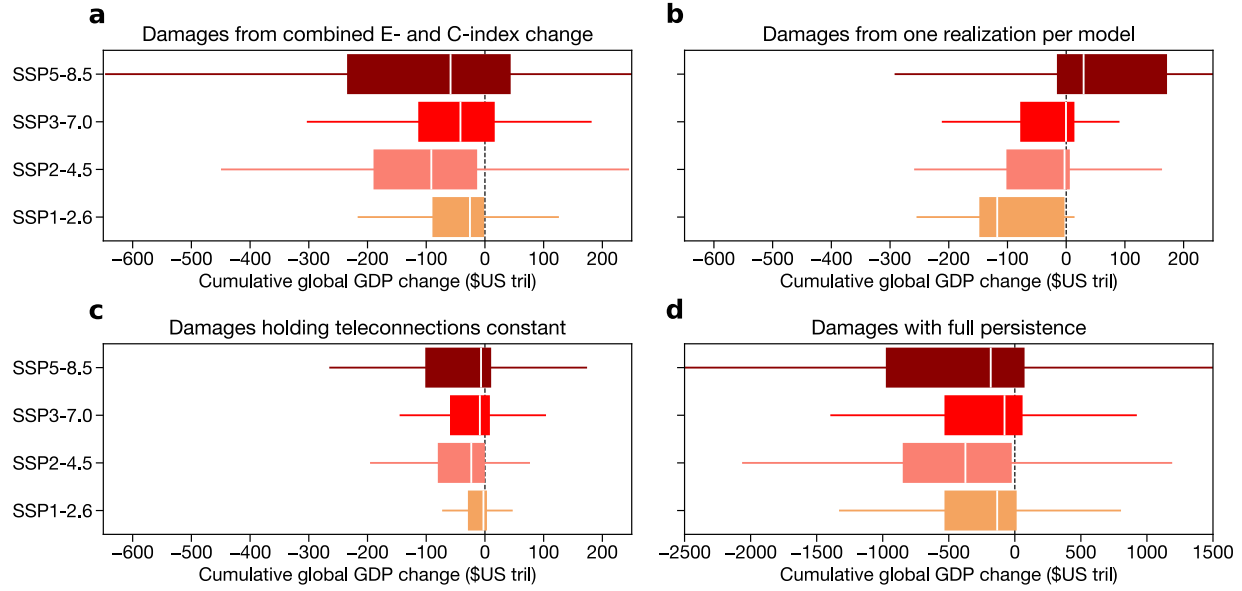


Fig. S13

Sensitivity of damage calculations to alternative choices. As in main text Fig. 4a, but for damages due to the combination of changes in E- and C-index amplitude and teleconnections (A), E-index damages using only the first realization from each model (B), E-index damages using amplitude change but holding teleconnections constant (C), and E-index damages when allowing damages to be permanently persistent (i.e., using the 5-lag model and assuming that the cumulative effects are never recovered) (D). All panels use a constant 2% discount rate.

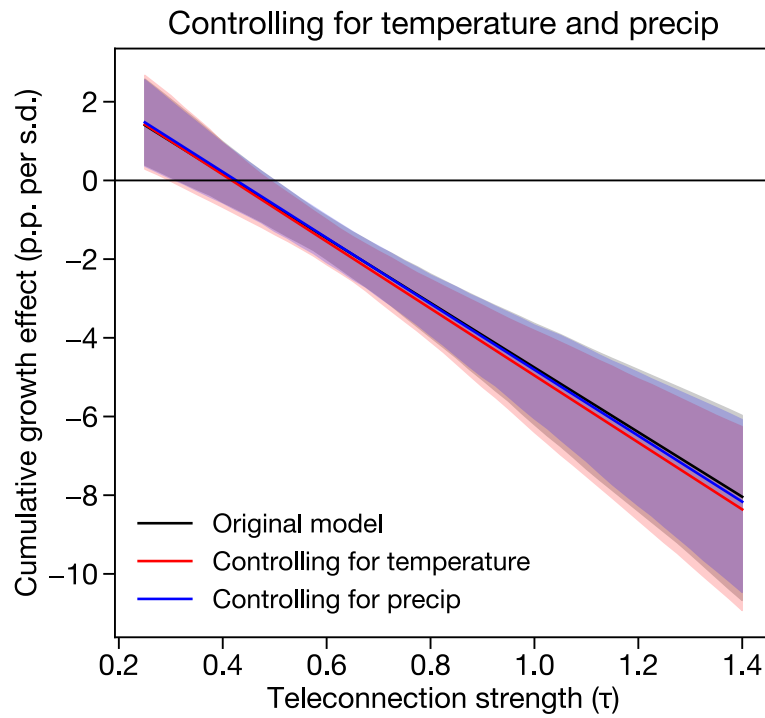


Fig. S14

Effects of controlling for temperature and precipitation in our regression model. Black line shows results from the original model, red line shows results with the addition of linear and quadratic terms for country-level annual mean temperature, and blue line shows results with the addition of linear and quadratic terms for the country-level annual average of monthly total precipitation. Shading shows the 95% confidence intervals from bootstrap resampling by country, as in the main analysis.

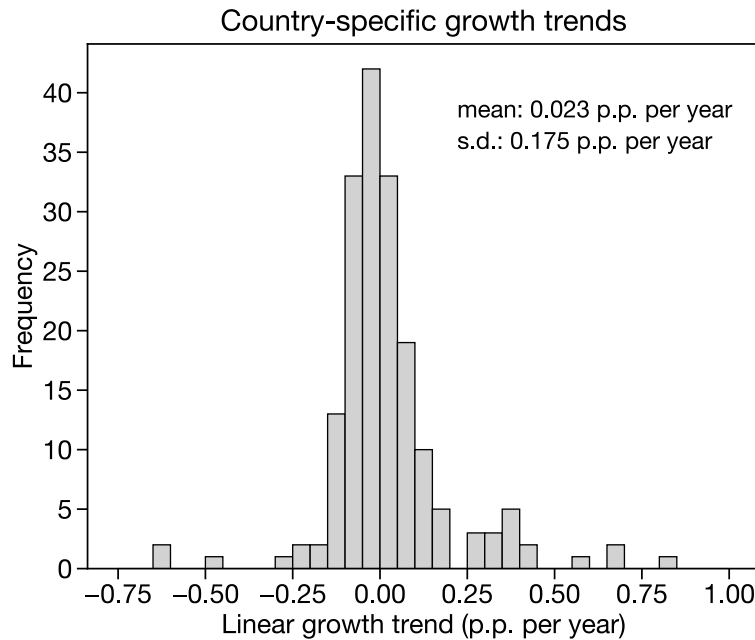


Fig. S15

Linear trends in growth. Growth trends are calculated as the linear coefficient on the univariate regression of each country's growth time series onto time. Only countries with 10 or more years of growth data are included in this histogram. Text in the top right denotes the mean and standard deviation of the distribution of trends across countries.

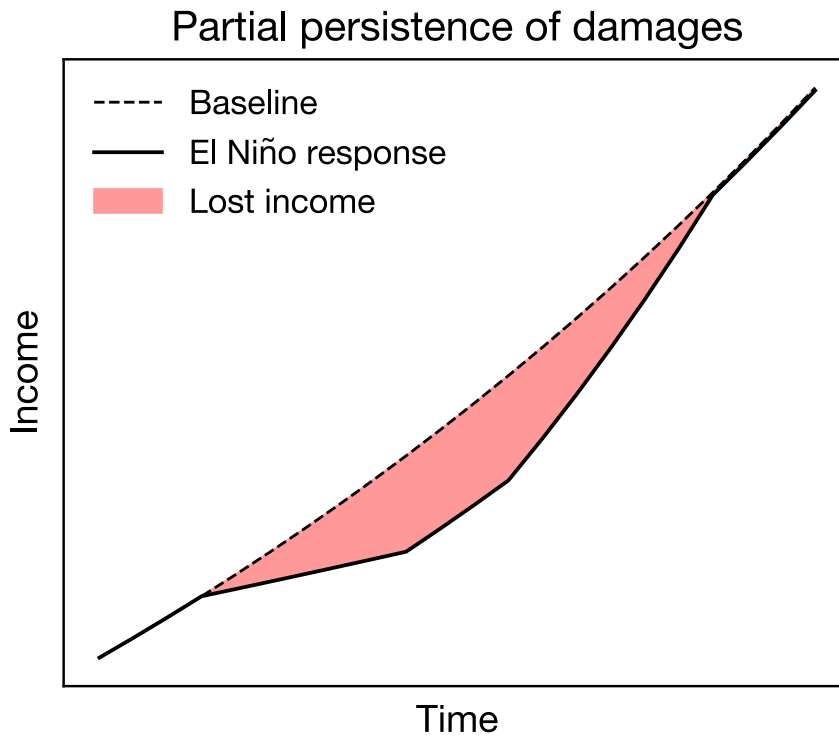


Fig. S16

Partial persistence of economic damages. This figure shows a schematic of how we implement the recovery period in our damage projections. El Niño events negatively affect growth in the year of the event and in the five years following the event, as in our main model. However, from years 9 to 14, we allow economies to recover back to their baseline economic trajectory. In the meantime, there is substantial lost income relative to that baseline trajectory, shown as the red shaded area.

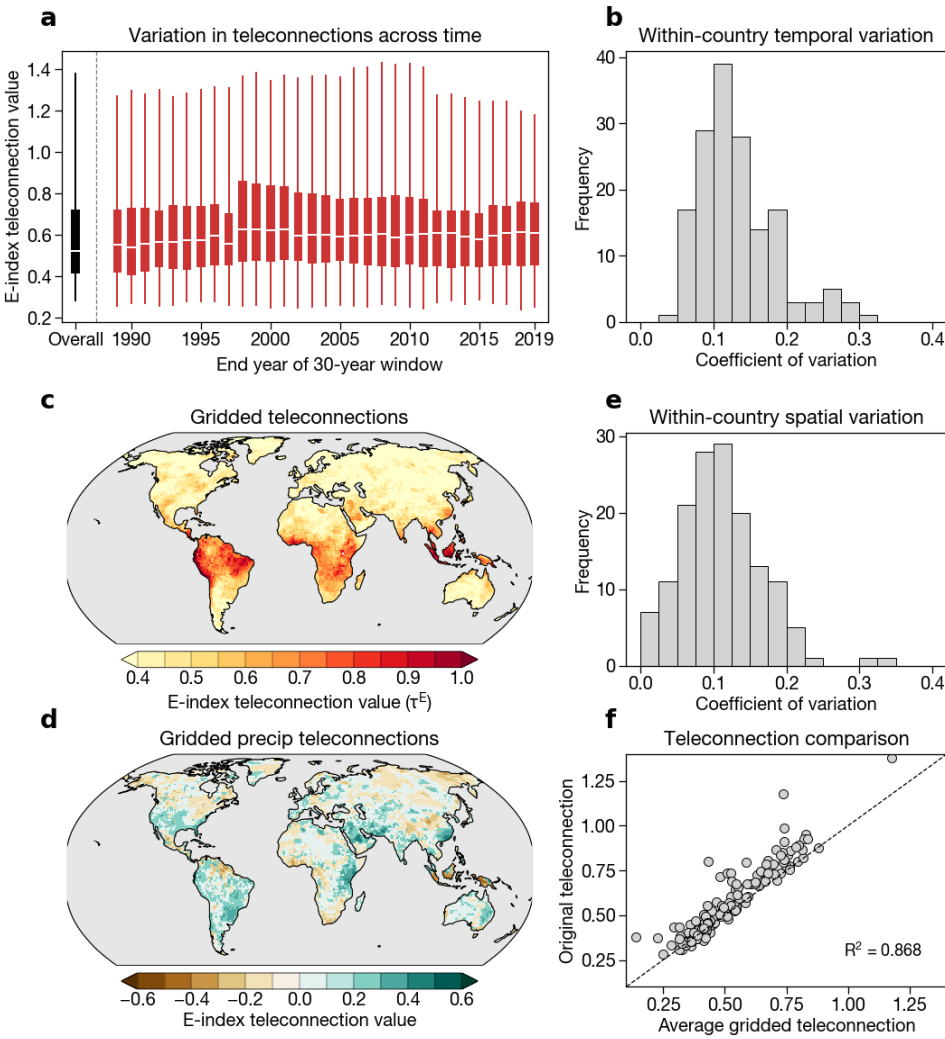


Fig. S17

Spatiotemporal heterogeneity of observed teleconnections. A) Distribution of E-index teleconnections in 30-year windows, with x-axis marking the final year of the 30-year window. An end year of 2015, for example, implies a start year of 1986. The black boxplot shows the original distribution of teleconnections calculated over the whole 1960-2019 period. White lines show medians, boxes extend to the 25th and 75th percentiles, and whiskers span the range of the data. B) Within-country temporal variation, calculated as the coefficient of variation over the 30-year windows shown in (A). This calculation is performed by dividing the standard deviation of each country's teleconnection values over all 30-year windows by its mean teleconnection over those windows. C) Grid-cell E-index teleconnections, calculated using the same method as the country-level teleconnections, but with standardized grid-cell temperature and precipitation data. D) Grid-cell precipitation teleconnections, meaning the precipitation component of (C). Note that the sign is preserved in (D), whereas the teleconnections in (C) and in the main analysis use absolute values. E) Within-country spatial variation in teleconnections, calculated as the coefficient of variation of the grid-cell teleconnections when aggregated to the country scale. F) Relationship between gridded teleconnections averaged at the country scale (with population weighting) and the original teleconnections using country-average temperature and precipitation.

Table S1.

E-index coefficients with alternative clustering techniques. E-index regression coefficients from the main regression model (Eqn. 1) using various parametric standard error clustering schemes. The marginal effect of the E-index for a country i is calculated as the main effect of the E-index plus the interaction term times $\tau_i^E (\beta + \theta * \tau_i^E)$, Eqn. 2). Clustering accounts for both spatiotemporal autocorrelation in errors as well as heteroskedasticity across clusters. In all models, the C-index terms and the country fixed effect are included but not shown in the table for simplicity.

	<i>Dependent variable: growth</i>				
	(1)	(2)	(3)	(4)	(5)
$E_t (\beta_0)$	0.0066*** (0.0016)	0.0066* (0.0033)	0.0066 (0.0035)	0.0066* (0.0025)	0.0066 (0.0041)
$E_{t-1} (\beta_1)$	0.0019 (0.0018)	0.0019 (0.0028)	0.0019 (0.0034)	0.0019 (0.0025)	0.0019 (0.0033)
$E_{t-2} (\beta_2)$	0.0054* (0.0022)	0.0054 (0.0044)	0.0054 (0.0043)	0.0054 (0.0041)	0.0054 (0.0039)
$E_{t-3} (\beta_3)$	0.0081*** (0.0021)	0.0081* (0.0036)	0.0081* (0.0035)	0.0081* (0.0029)	0.0081* (0.0032)
$E_{t-4} (\beta_4)$	0.0053** (0.0019)	0.0053 (0.0033)	0.0053* (0.0026)	0.0053* (0.0020)	0.0053* (0.0023)
$E_{t-5} (\beta_5)$	0.0064** (0.0021)	0.0064* (0.0031)	0.0064* (0.0030)	0.0064** (0.0014)	0.0064* (0.0031)
$E_t \times \tau_i^E (\Theta_0)$	-0.0163*** (0.0028)	-0.0163** (0.0055)	-0.0163*** (0.0042)	-0.0163** (0.0036)	-0.0163** (0.0051)
$E_{t-1} \times \tau_i^E (\Theta_1)$	-0.0072* (0.0028)	-0.0072 (0.0039)	-0.0072 (0.0043)	-0.0072 (0.0030)	-0.0072 (0.0047)
$E_{t-2} \times \tau_i^E (\Theta_2)$	-0.0158*** (0.0036)	-0.0158** (0.0059)	-0.0158*** (0.0048)	-0.0158* (0.0061)	-0.0158*** (0.0046)
$E_{t-3} \times \tau_i^E (\Theta_3)$	-0.0169*** (0.0032)	-0.0169*** (0.0050)	-0.0169*** (0.0042)	-0.0169** (0.0036)	-0.0169*** (0.0038)
$E_{t-4} \times \tau_i^E (\Theta_4)$	-0.0123*** (0.0032)	-0.0123** (0.0045)	-0.0123*** (0.0029)	-0.0123** (0.0024)	-0.0123*** (0.0025)
$E_{t-5} \times \tau_i^E (\Theta_5)$	-0.0121*** (0.0034)	-0.0121* (0.0048)	-0.0121*** (0.0035)	-0.0121*** (0.0010)	-0.0121*** (0.0035)
Observations	7183	7183	7183	7183	7183
Clustering	Country	Year-continent	Year	Continent	Five-year block

*** $p < 0.001$; ** $p < 0.01$; * $p < 0.05$

Table S2.

C-index coefficients with alternative clustering techniques. C-index regression coefficients from the main regression model (Eqn. 1) using various parametric standard error clustering schemes. The marginal effect of the C-index for a country i is calculated as the main effect of the C-index plus the interaction term times $\tau_i^C (\phi + \Psi * \tau_i^C)$, Eqn. 2). Clustering accounts for both spatiotemporal autocorrelation in errors as well as heteroskedasticity across clusters. In all models, the E-index terms and the country fixed effect are included but not shown in the table for simplicity.

	<i>Dependent variable: growth</i>				
	(1)	(2)	(3)	(4)	(5)
$C_t (\Phi_0)$	−0.0038*	−0.0038	−0.0038	−0.0038	−0.0038
	(0.0016)	(0.0028)	(0.0032)	(0.0015)	(0.0052)
$C_{t-1} (\Phi_1)$	0.0048***	0.0048	0.0048	0.0048	0.0048
	(0.0013)	(0.0043)	(0.0044)	(0.0020)	(0.0041)
$C_{t-2} (\Phi_2)$	0.0021	0.0021	0.0021	0.0021	0.0021
	(0.0012)	(0.0036)	(0.0042)	(0.0009)	(0.0021)
$C_{t-3} (\Phi_3)$	0.0028**	0.0028	0.0028	0.0028	0.0028
	(0.0010)	(0.0033)	(0.0039)	(0.0014)	(0.0027)
$C_{t-4} (\Phi_4)$	−0.0015	−0.0015	−0.0015	−0.0015	−0.0015
	(0.0013)	(0.0035)	(0.0040)	(0.0011)	(0.0021)
$C_{t-5} (\Phi_5)$	−0.0031*	−0.0031	−0.0031	−0.0031***	−0.0031
	(0.0015)	(0.0026)	(0.0032)	(0.0004)	(0.0042)
$C_t \times \tau_i^C (\Psi_0)$	0.0026	0.0026	0.0026	0.0026	0.0026
	(0.0023)	(0.0039)	(0.0042)	(0.0017)	(0.0067)
$C_{t-1} \times \tau_i^C (\Psi_1)$	−0.0074***	−0.0074	−0.0074	−0.0074	−0.0074
	(0.0018)	(0.0056)	(0.0051)	(0.0031)	(0.0047)
$C_{t-2} \times \tau_i^C (\Psi_2)$	−0.0059**	−0.0059	−0.0059	−0.0059**	−0.0059*
	(0.0018)	(0.0047)	(0.0048)	(0.0011)	(0.0026)
$C_{t-3} \times \tau_i^C (\Psi_3)$	−0.0041**	−0.0041	−0.0041	−0.0041*	−0.0041
	(0.0015)	(0.0044)	(0.0046)	(0.0013)	(0.0034)
$C_{t-4} \times \tau_i^C (\Psi_4)$	0.0005	0.0005	0.0005	0.0005	0.0005
	(0.0019)	(0.0047)	(0.0046)	(0.0012)	(0.0028)
$C_{t-5} \times \tau_i^C (\Psi_5)$	0.0025	0.0025	0.0025	0.0025*	0.0025
	(0.0020)	(0.0035)	(0.0034)	(0.0007)	(0.0045)
Observations	7183	7183	7183	7183	7183
Clustering	Country	Year-continent	Year	Continent	Five-year block

*** $p < 0.001$; ** $p < 0.01$; * $p < 0.05$

Table S3.

CMIP6 models and realizations used from the SSP1-2.6 scenario. Monthly sea surface temperature (“tos”), monthly atmospheric temperature (“tas”), and daily precipitation (“pr”) are used from each model. Bolded models are those that have at least 1 realization selected for the final analysis (Methods).

Model	Total realizations	Selected realizations
CanESM5	50	0
KACE-1-0-G	3	0
MIROC-ES2L	7	7
MIROC6	50	50
MRI-ESM2-0	5	4

Table S4.

CMIP6 models and realizations used from the SSP2-4.5 scenario. Monthly sea surface temperature (“tos”), monthly atmospheric temperature (“tas”), and daily precipitation (“pr”) are used from each model. Bolded models are those that have at least 1 realization selected for the final analysis (Methods).

Model	Total realizations	Selected realizations
ACCESS-CM2	3	0
ACCESS-ESM1-5	11	0
CAMS-CSM1-0	1	0
CESM2	2	0
CESM2-WACCM	3	2
CMCC-CM2-SR5	1	1
CMCC-ESM2	1	1
CNRM-CM6-1	1	0
CanESM5	50	0
EC-Earth3	8	8
FGOALS-g3	3	0
GFDL-ESM4	1	0
HadGEM3-GC31-LL	1	0
INM-CM4-8	1	0
INM-CM5-0	1	0
IPSL-CM6A-LR	5	0
KACE-1-0-G	3	0
MIROC-ES2L	30	30
MIROC6	33	33
MPI-ESM1-2-HR	2	1
MPI-ESM1-2-LR	10	9
NorESM2-LM	2	0
NorESM2-MM	2	1
UKESM1-0-LL	5	0

Table S5.

CMIP6 models and realizations used from the SSP3-7.0 scenario. Monthly sea surface temperature (“tos”), monthly atmospheric temperature (“tas”), and daily precipitation (“pr”) are used from each model. Bolded models are those that have at least 1 realization selected for the final analysis (Methods).

Model	Total realizations	Selected realizations
ACCESS-CM2	3	0
ACCESS-ESM1-5	10	0
CAMS-CSM1-0	1	0
CESM2	2	0
CESM2-WACCM	1	1
CMCC-CM2-SR5	1	1
CMCC-ESM2	1	1
CNRM-CM6-1	1	0
CanESM5	50	0
FGOALS-g3	4	0
GFDL-ESM4	1	0
INM-CM4-8	1	0
INM-CM5-0	5	0
IPSL-CM6A-LR	5	0
KACE-1-0-G	3	0
MIROC-ES2L	10	10
MIROC6	3	3
MPI-ESM1-2-HR	10	4
MPI-ESM1-2-LR	7	6
MRI-ESM2-0	5	5
NorESM2-LM	1	1
NorESM2-MM	1	1
UKESM1-0-LL	13	0

Table S6.

CMIP6 models and realizations used from the SSP5-8.5 scenario. Monthly sea surface temperature (“tos”), monthly atmospheric temperature (“tas”), and daily precipitation (“pr”) are used from each model. Bolded models are those that have at least 1 realization selected for the final analysis (Methods).

Model	Total realizations	Selected realizations
ACCESS-CM2	2	0
ACCESS-ESM1-5	6	0
CAMS-CSM1-0	1	0
CESM2	0	0
CESM2-WACCM	3	1
CMCC-CM2-SR5	1	1
CMCC-ESM2	1	1
CNRM-CM6-1	1	0
CanESM5	50	0
FGOALS-g3	3	0
GFDL-ESM4	1	0
HadGEM3-GC31-LL	4	0
HadGEM3-GC31-MM	4	0
INM-CM4-8	1	0
INM-CM5-0	1	0
IPSL-CM6A-LR	4	0
KACE-1-0-G	3	0
MIROC-ES2L	1	1
MIROC6	50	50
MPI-ESM1-2-HR	2	1
NorESM2-LM	1	1
NorESM2-MM	1	1
UKESM1-0-LL	5	0

Table S7.

Correlation matrix for the E-index and its lags. Each table entry shows the Pearson correlation coefficient between the E-index at various time lags and the E-index at each other time lag.

	E_t	E_{t-1}	E_{t-2}	E_{t-3}	E_{t-4}	E_{t-5}
E_t		-0.101	-0.335	0.002	0.034	0.002
E_{t-1}			-0.092	-0.336	-0.01	0.037
E_{t-2}				-0.089	-0.291	-0.029
E_{t-3}					-0.094	-0.291
E_{t-4}						-0.076